NJC

PAPER

View Article Online
View Journal | View Issue

Cite this: *New J. Chem.*, 2019, **43**, 17872

V(v)-Schiff base species induce adipogenesis through structure-specific influence of genetic targets†

O. Tsave, [a] E. Halevas, [a] M. P. Yavropoulou, [b] E. Yovos, [b] A. Hatzidimitriou, [c] V. Psycharis, [d] K. Ypsilantis, [e] P. Stathi [f] and A. Salifoglou *[a]

Vanadium has been known to exhibit numerous functions in biological systems, projecting exogenous activity linked to regulatory roles in cell metabolism and insulin mimesis. Poised to probe into the vanadium adipogenic potential, reflecting on efficient anti-diabetic drugs, research was launched in our labs to pursue the (a) synthesis of diversely structured Schiff base ligands, as vanadium chelating binders, containing a variably configured *o*-vanillin core with a specified common organic *o*-aminophenol tether, (b) synthesis of a family of well-defined soluble vanadium-Schiff base compounds, bearing the above mentioned Schiff ligands (and in one case 4,4′-bipyridine), (c) study of their toxicity profile and adipogenic activity in 3T3-L1 fibroblasts toward mature adipocytes, and (d) determination of molecular biological targets linked to the vanadium-induced cell differentiation process, thereby unravelling factors impacting signaling pathways influencing insulin mimesis. The results suggest that (a) all emerging vanadospecies contain V(v) mononuclear centers bound to Schiff bases (and 4,4′-bipyridine), (b) a well-defined (solid-state and solution) physicochemical profile of all species justifies their selection in biological studies, (c) the vanadium toxicity profile is strongly related to the form of V(v) (complexed forms, substrate-ligand nature), (d) there is a structure-specific behavior of vanadium influencing adipogenesis, and (e) molecular target loci are also influenced by vanadoforms in a structure-specific fashion, thereby collectively projecting an interwoven role of factors emanating from vanadium and impacting cell differentiation and insulin mimetic activity. The so far accrued knowledge constitutes the basis for further development of biomarker-driven structure-specific vanadodrugs, contributing through insulin biomimicry to therapeutic technologies in Diabetes mellitus.

Received 16th May 2019,
Accepted 15th October 2019

DOI: 10.1039/c9nj02520k

rsc.li/njc

1. Introduction

Diabetes mellitus (DM) is one of the most common endocrine disorders. It is estimated that in 2018 there were more than 500 million certified cases of type 2 diabetes worldwide, with the onset of the disease expected to rise dramatically in the upcoming years.[1] DM can be divided into several clinically distinct types. Broadly, there are two major types, type 1 diabetes (T1D) and type 2 diabetes (T2D), according to the etiopathology of the disorder. T2D appears to be the most common form of diabetes (90% of all diabetic patients), mainly characterized by insulin resistance, whereas T1D is an autoimmune disorder.[2] In all cases, insulin serves as the key factor with abnormal secretion and/or action. Insulin deficiency results in elevated blood glucose levels (hyperglycemia) and impaired metabolism of carbohydrates, fat, and proteins, among others, and is strongly related to usually severe secondary complications (cardiovascular disease, diabetic neuropathy, *etc.*). Current treatment pathways of

[a] *Laboratory of Inorganic Chemistry and Advanced Materials, Department of Chemical Engineering, Aristotle University of Thessaloniki, Thessaloniki 54124, Greece. E-mail: salif@auth.gr; Fax: +30-2310-996-196; Tel: +30-2310-996-179*
[b] *Division of Clinical and Molecular Endocrinology, 1st Department of Internal Medicine, AHEPA, University Hospital, Aristotle University of Thessaloniki, Thessaloniki 54124, Greece*
[c] *Laboratory of Inorganic Chemistry, Department of Chemistry, Aristotle University of Thessaloniki, Thessaloniki 54124, Greece*
[d] *Institute of Nanoscience and Nanotechnology, NCSR "Demokritos", Aghia Paraskevi 15310, Attiki, Greece*
[e] *Department of Chemistry, University of Ioannina, Ioannina 45110, Greece*
[f] *Laboratory of Physical Chemistry of Materials & Environment, Department of Physics, University of Ioannina, Ioannina 45110, Greece*

† Electronic supplementary information (ESI) available. CCDC 1914116 (**1**), 1898796 (**2**), 1898797 (**3**), and 1898798 (**4**). For ESI and crystallographic data in CIF or other electronic format see DOI: 10.1039/c9nj02520k

DM are based either on exogenous insulin and/or hypoglycemic agents.[3,4] Although these therapeutic approaches are well-established, they have several limitations, including significant side-effects and elevated levels of patient stress. To this end, extensive efforts have been made over the past few decades to investigate the insulin mimetic effect of a plethora of agents (natural products, metal ions, organic extracts, *etc.*) that could enhance or even displace insulin use in treating or alleviating DM symptoms.[5–7]

The first report on therapeutic applications of vanadium compounds in humans appeared very early in 1899. However, it was not until 1980 that the insulin-mimetic effect of vanadium was discovered.[8,9] The effect pertains to the ability of vanadium salts and vanadium complexes to lower blood glucose levels by triggering cellular glucose uptake for further catabolism. It is worth mentioning that although simple vanadium salts, such as $NaVO_3$ and $VOSO_4$, can lower blood glucose levels in rats and humans, numerous studies have shown that hybrid vanadium-organic substrate complexes are less toxic and several times more effective in lowering blood glucose levels.[10,11] What was considered a critical step toward the use of vanadium as a potent anti-diabetic agent in those early studies was the development of vanadium complexes that would have increased bioavailability, such that lower doses could improve efficacy and safety. As such, considerable research has gone into studying the active form of insulin-mimetic vanadium complexes, their pharmacological properties and their transport to target sites in the body by the blood stream. Vanadium complexes show insulin-mimetic effects in three oxidation states [V(III), V(IV) and V(V)]. Vanadium(V)-oxido anions and complexes are known to inhibit protein tyrosine phosphatases (PTPs).[12] Inhibition of PTPs keeps the insulin receptor phosphorylated, allowing glucose transport into the cell. Under physiological conditions, vanadium complexes can interconvert between V(IV) and V(V), and V(V) can inhibit PTPs.[13] Moreover, V(IV) can activate the recruitment of glucose transporters to the cell membrane, thereby increasing glucose cell uptake and lowering blood glucose levels.[14]

Given the fact that insulin exerts its properties in multiple ways (cell proliferation, differentiation, growth, gene expression, *etc.*) insulin mimesis of candidate agents can also be studied toward these actions.[15] Adipogenesis is an intimately linked part of metabolism, defined as a highly complex physiological process, by which precursor stem cells undergo differentiation to form mature adipocytes.[16] In mammals, energy is mainly stored in the form of fat in the adipose tissue, which serves as a source on-demand.[17] Adipose tissue is characterized as a highly metabolic endocrine organ and hence adipose tissue is considered as a key component in the investigation of such relevant (patho)physiologies in insulin resistance and hence Diabetes mellitus II (T2D).

Taking into account that antidiabetic candidate drugs should (a) exhibit atoxicity, (b) optimal insulin mimetic activity, and (c) enhanced ability to cross membrane barriers in their effort to deliver their active cargo, organic substrates appear to play a significant role, thereby attracting considerable interest as potential V(IV,V) binders. One such family of organic substrates includes Schiff bases. They are simple organic ligands, emulating a significant number of natural substrates of variable mass and (bio)chemical reactivity, while concurrently possessing a diverse spectrum of structural features, enabling them to pursue effective interactions with metal ions.[18–20] Suffice to state that they have been studied extensively as compounds exhibiting a variable spectrum of biological activities linked to industrial, antifungal, antibacterial, anticancer, antidiabetic, antiviral and herbicidal applications.[21–31]

Guided by the idea that appropriately designed Schiff bases might effectively bind V(IV,V) ions, thereby formulating the biological profile of those metal ions with respect to insulin mimesis, efforts were launched to (a) design and synthesize diversely composed Schiff bases, bearing the common 2-aminophenol component, promoting vanadium complexation through distinctly structured anchor groups, (b) pursue the synthesis of binary and/or ternary complex assemblies of such Schiff base ligands with vanadium and ancillary binders, (c) investigate their insulin mimetic potency toward cellular differentiation of premature fibroblasts toward mature fibroblasts capable of taking up glucose, (d) study the interactions of the arising vanadium species with cellular molecular targets intimately linked to insulin-induced signaling pathways promoting glucose uptake, and finally (e) configure biological profiles, thus allowing identification of structure-specific speciation leading to efficient insulin mimetic processes. On these grounds, the herein described research pertains to (a) systematic efforts leading to binary–ternary vanadium(V)-Schiff base complex compounds and their physicochemical characterization, and (b) molecular biological studies exemplifying biochemical profiles enabling meaningful correlations with structural features, collectively contributing to the understanding of vanadium insulin-mimesis and its potential use through metallodrugs in the treatment of diabetes.

2. Results and discussion

2.1 Synthesis

Synthetic exploration of the binary V(V)-Schiff base systems in this work followed carefully designed approaches. The employed ligands $\mathbf{L_1H_2}$–$\mathbf{L_3H_2}$ were synthesized through Schiff base condensation reactions involving *o*-vanillin and 2-aminophenol ($\mathbf{L_1H_2}$), salicylaldehyde and 2-aminophenol ($\mathbf{L_2H_2}$), and 2-hydroxy-1-naphthaldehyde and 2-aminophenol ($\mathbf{L_3H_2}$).[32–34] Subsequently, the $[VO(L_1)(OCH_3)(CH_3OH)]$ (**1**) complex was synthesized in a facile fashion from simple reagents in alcoholic solutions. In a typical reaction, $[VO(C_5H_7O_2)_2]$ reacted with the Schiff base $\mathbf{L_1H_2}$ using methanol as a solvent. The overall stoichiometric reaction leading to **1** is shown schematically below:

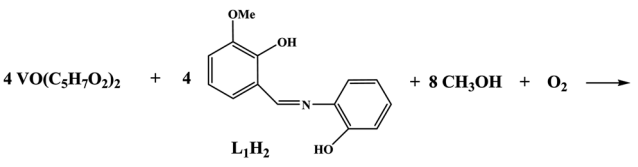

Similarly, $[VO(C_5H_7O_2)_2]$ reacted with Schiff base $\mathbf{L_1H_2}$ in methanol, in the presence of 4,4′-bipyridine. The stoichiometric reaction leading to the formation of compound $[VO(L_1)(CH_3O)](C_{10}H_8N_2)[VO(L_1)(CH_3O)]$ (**2**) is shown below:

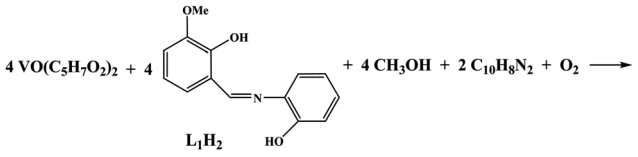

$$2\,[VO(L_1)(CH_3O)](C_{10}H_8N_2)[VO(L_1)(CH_3O)] + 8\,C_5H_8O_2 + 2\,H_2O$$

In an analogous reaction, $[VO(C_5H_7O_2)_2]$ reacted with Schiff base $\mathbf{L_2H_2}$ in methanol. The stoichiometric reaction leading to the formation of $[VO(L_2)(OCH_3)(CH_3OH)]$ (**3**) is shown below:

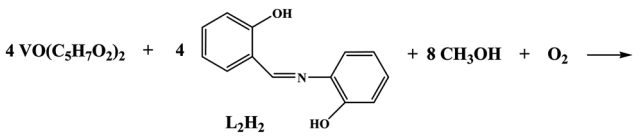

$$4\,[VO(L_2)(CH_3O)(CH_3OH)] + 8\,C_5H_8O_2 + 2\,H_2O$$

In a similar reaction, $[VO(C_5H_7O_2)_2]$ reacted with Schiff base $\mathbf{L_3H_2}$ in methanol, in the presence of sodium hydroxide. The stoichiometric reaction leading to the formation of compound $[\{VO_2\}(L_3)]Na$ (**4**) is shown below:

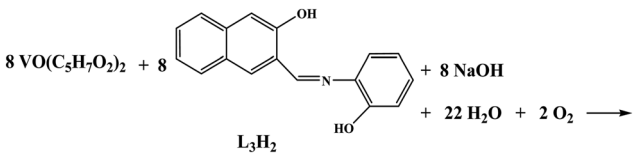

$$2\,[VO_2(L_3)Na(H_2O)_2VO_2(L_3)Na(H_2O)_3]_2 \cdot H_2O + 16\,C_5H_8O_2 + 4\,H_2O$$

Diethyl ether was added as a precipitating solvent to the reaction mixture in the first and second reactions described above. The third and fourth reaction mixtures were allowed to evaporate slowly. Brown crystalline materials emerged in all four reactions described above, the analytical composition of which was consistent with the formulation in **1–4**, respectively (*vide supra*). Positive identification of the crystalline products was achieved by elemental analysis, FT-IR spectroscopic methods and X-ray crystallographic determination for isolated single crystals from **1–4**. All complexes are stable in the crystalline form, in air, for fairly long periods of time. All four species are readily dissolved in water and DMSO, less soluble in CH_3OH and acetone, sparingly soluble in i-PrOH, and insoluble in acetonitrile and chloroform at room temperature.

The common feature of all members in the Schiff base series was the *o*-aminophenol moiety, ultimately providing vanadium binders $\mathbf{L_1H_2}$, $\mathbf{L_2H_2}$, and $\mathbf{L_3H_2}$. Progressive modification of ligand nature led to synthetic efforts in methanolic reaction mixtures under specific conditions, guided by reagent molecular stoichiometries, finally affording isolable crystalline materials **1–4**.

2.2 Physicochemical characterization

2.2.1 X-ray crystallographic structures. The X-ray crystal structures of **1–4** reveal discrete solid-state lattices. Crystal structure information is provided in Table 1, with molecular structures of **1–4** given in Fig. 1–4, respectively; selected bond distances and angles are listed in Table 2. Compound **1** crystallizes in the monoclinic space group $P2_1/a$. In the asymmetric unit, there exist $[VO(L_1)(OCH_3)(CH_3OH)]$ assemblies with the molecular structure presented in Fig. 1. The vanadium centers in the aforementioned assemblies are six coordinate, with an NO_5 environment generating a distorted octahedral coordination geometry. Two of the oxygen atoms are provided by the deprotonated L_1 ligand and three are from the methoxy, methanol and oxido ligands. The axial V–O(22) bond (trans to the V=O bond) is longer than the equatorial bonds due to the trans effect.[35] In the equatorial plane, the Schiff base is coordinated to the V center through five- and six-membered chelate rings, with bite angles 77.4° (O(1)–V–N) and 83.5° (O(2)–V–N), respectively. The other oxygen-containing bond lengths follow the trend observed in similar compounds with an NO_5 environment around vanadium.[36] The complex assemblies in **1** through the O(22)–H(22)O···O(1)′ hydrogen bonds (O–H: 0.73, H···O(1)′: 2.08, O(22)···O(1)′: 2.752 Å and O(22)–H(22)O···O(1)′: 153°; symmetry code: $x - 1/2$, $-y + 1/2$, z) form chains parallel to the *a* crystallographic axis (Fig. S1, ESI†). These chains interact through shifted π–π interactions of $[\mathbf{L_1}]^{2-}$ ligands, thus forming layers parallel to the (001) crystallographic plane (Fig. S1, ESI†). The centroid–centroid distanses take on values of 3.778 and 4.048 Å (indicated with dark red and orange dashed lines, respectively, in Fig. S1, ESI†).

Compound **2** crystallizes in the triclinic space group $P\bar{1}$. In the unit cell there exist dinuclear complex $[VO(L_1)(CH_3O)](C_{10}H_8N_2)[VO(L_1)(CH_3O)]$ assemblies, bearing a unit molecular structure presented in Fig. 2. The complexes are centrosymmetric, with the inversion center located at the middle of the distance of the sigma bond in the 4,4′-bipyridine ligand.

Vanadium (V(v)) cations are again six coordinate, exhibiting an O_4N_2 environment and a distorted octahedral geometry. Two of the oxygen atoms are provided by the doubly deprotonated $[\mathbf{L_1}]^{2-}$ ligand, with an additional two oxygens originating from the methoxy and oxido ligands. One of the nitrogen atoms (N(1)) is from $[\mathbf{L_1}]^{2-}$, with the second one (N(2)) belonging to the 4,4′-bipyridine ligand. The axial bond length V–N(2) is 2.4772(19) Å, considerably longer than the rest of the equatorial bonds due to the trans effect (trans to the V=O(3) bond). The coordination geometry of the 4,4′-bipyridine ligand is strange, as the metal cation is shifted from the ligand mean plane by 0.864 Å and the angle V–N(2)–C(17) is 161.86°. The doubly deprotonated Schiff base is coordinated to the vanadium center V(v) in a chelate tridentate mode through one five-membered and one six-membered ring, with bite angles of 77.08° (O(1)–V(1)–N(1)) and 83.03° (O(2)–V(1)–N(1)), respectively. The rest of the vanadium–oxygen bond lengths are quite similar to those observed in analogous complexes.[37] No hydrogen bonding or other type of intermolecular or intramolecular interaction was found in the crystal structure.

Table 1 Crystallographic data for compounds $[VO(L_1)(CH_3O)(CH_3OH)]$ (**1**), $[VO(L_1)(CH_3O)](C_{10}H_8N_2)[VO(L_1)(CH_3O)]$ (**2**), $[VO(L_2)(CH_3O)(CH_3OH)]$ (**3**), and $[VO_2(L_3)Na(H_2O)_2VO_2(L_3)Na(H_2O)_3]_2{\cdot}H_2O$ (**4**)

Compound	1	2	3	4
Chemical formula	$C_{16}H_{18}NO_6V$	$C_{20}H_{18}N_2O_5V$	$C_{15}H_{16}NO_5V$	$C_{68}H_{66}N_4Na_4O_{27}V_4$
M_r	371.25	417.31	341.24	1667.01
Crystal system	Monoclinic	Triclinic	Monoclinic	Monoclinic
Space group	$P2_1/a$	$P\bar{1}$	$P2_1/n$	$P2_1/n$
Temperature (K)	160	295	295	299
a (Å)	7.1228 (1)	7.9698 (8)	7.2356 (4),	7.3508 (5),
b (Å)	22.3349 (5)	10.5539 (11)	21.3942 (13)	21.9513 (15)
c (Å)	10.4326 (2)	11.3860 (12)	19.5771 (13)	21.7346 (17)
α (°)	90	98.204 (3)	90	90
β (°)	100.566 (1)	99.184 (3)	100.594 (4)	92.504 (4)
γ (°)	90	90.805 (4)	90	90
V (Å^3)	1631.55 (5)	935.09 (10)	2978.9 (3)	3503.7 (4)
Z	4	2	8	2
Radiation type	Cu Kα	Mo Kα	Mo Kα	Mo Kα
μ (mm^{-1})	5.38	0.57	0.69	0.63
T_{min}, T_{max}	0.549, 1.000	0.91, 0.92	0.86, 0.91	0.97, 0.97
No. of reflections				
Measured	10 727	11 781	46 827	58 024
Independent	2642	7021	5992	7682
Observed [$I > 2.0\sigma(I)$]	2100	3498	4139	5051
R_{int}	0.050	0.025	0.057	0.016
$(\sin\theta/\lambda)_{max}$ (Å^{-1})	0.588	0.770	0.626	0.648
Refinement				
$R[F^2 > 2\sigma(F^2)]$	0.051	0.044	0.052	0.049
$R_w(F^2)$	0.134	0.106	0.112	0.097
S	1.05	1.00	1.00	1.00
No. of parameters	253	253	397	487
$\Delta\rho_{max}$, $\Delta\rho_{min}$ (e Å^{-3})	0.51, −0.48	0.60, −0.38	0.67, −0.42	0.50, −0.71

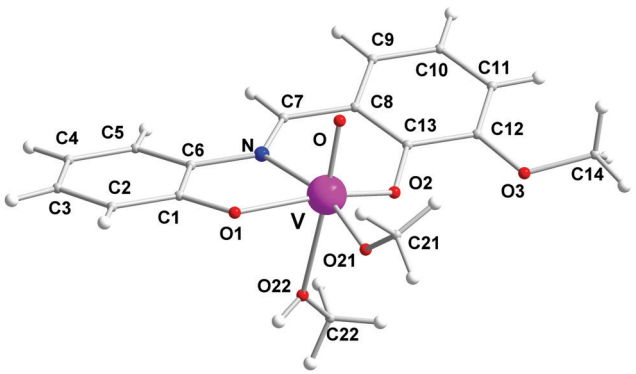

Fig. 1 Partially labeled plot of the molecular structure of compound **1**.

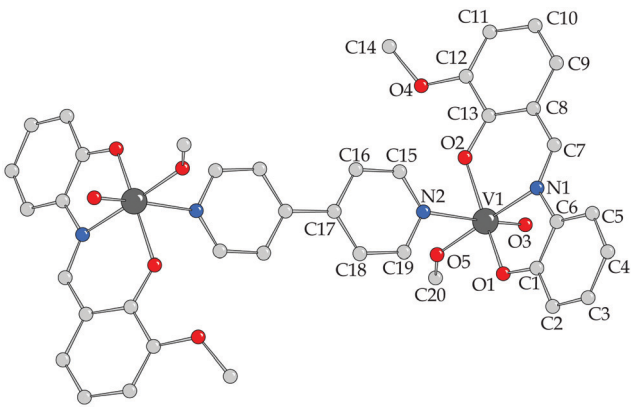

Fig. 2 Partially labeled plot of the molecular structure of **2**.

Compound **3** crystallizes in the monoclinic space group $P2_1/n$. In the asymmetric unit there are two slightly different complex assemblies bearing the formula $[VO(L_2)(CH_3O)(CH_3OH)]$. Fig. 3 presents the molecular structure of one of the two molecules. It is evident that the structures of compounds **1** and **3** are nearly similar. Bond lengths and angles are listed in Table 2. Vanadium (V(v)) cations are six coordinate, similar to the corresponding center in **1**, with the same O_5N chromophore and a distorted octahedral geometry. Two of the oxygen atoms are provided by the doubly deprotonated $[\mathbf{L_2}]^{2-}$ ligand, with an additional three oxygens originating from the methoxy, methanol and oxido ligands. The axial, V–O(5) bond (trans to the V═O(3) bond), is longer than the equatorial bonds due to the trans effect. In the equatorial plane, the Schiff base is coordinated to the V(v) center through five and six-membered chelate rings, with bite angles 76.90° and 77.69° (O(1)–V(1)–N(1) and O(6)–V(2)–N(2)), respectively, and 84.69° and 84.27° for O(2)–V(1)–N(1) and O(7)–V(2)–N(2), respectively. All bond lengths follow the trend observed in similar compounds exhibiting an O_xN_y (where $x + y = 6$) environment around the vanadium center.[37] Hydrogen bonds arise from the coordinated methanol oxygen atoms to phenolic oxygen atoms from neighboring molecules, thus forming chains parallel to the a crystallographic axis (Fig. S2 in cyan lines, ESI†). These chains interact through shifted π–π interactions of $[\mathbf{L_2}]^{2-}$ ligands, thus forming layers parallel to the

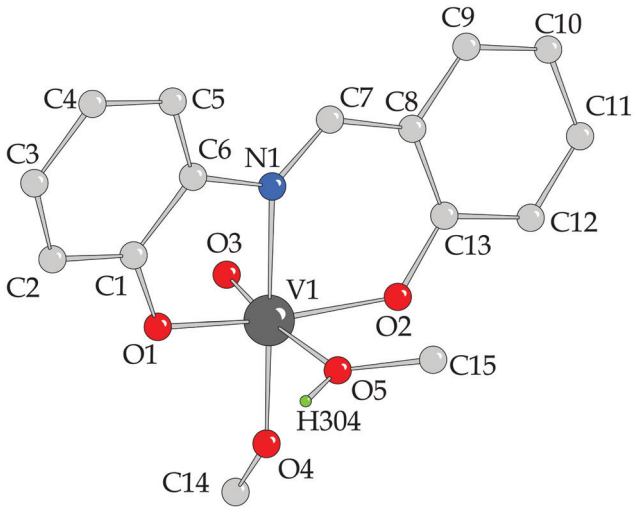

Fig. 3 Partially labeled plot of the molecular structure of compound **3**.

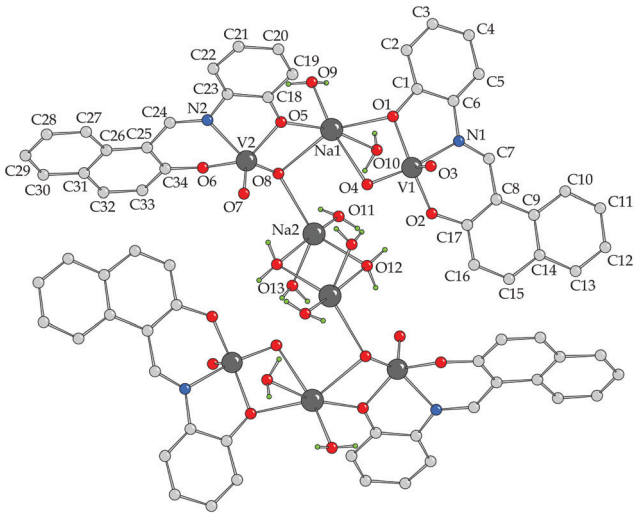

Fig. 4 Partially labeled plot of the molecular structure of compound **4**.

(001) crystallographic plane (Fig. S2, ESI†). The centroid–centroid distanses take up values 3.806 and 3.909 Å (indicated by violet lines in Fig. S2, ESI†).

Compound **4** crystallizes in the monoclinic space group $P2_1/n$. The asymmetric unit contains one centrosymmetric bimetallic octanuclear complex bearing the formula $C_{68}H_{64}N_4Na_4O_{26}V_4$ and one lattice water molecule. Fig. 4 shows the structure of $[VO_2(L_3)Na(H_2O)_2VO_2(L_3)Na(H_2O)_3]_2{\cdot}H_2O$. Bond lengths and angles are listed in Table 2. Vanadium (V(v)) cations as parts of the dioxidovanadium(v) (VO_2^+) units were found to be five coordinate with an O_4N chromophore. The trigonality index τ values are equal to 0.101 and 0.187 (close to zero) for V(1) and V(2), respectively. This indicates a distorted tetragonal pyramidal geometry around the vanadium centers. Two of the oxygen atoms in the coordination sphere of the vanadium cations are provided by the doubly deprotonated $[\mathbf{L_3}]^{2-}$ ligands, with another two oxygens coming from oxido ligands. All bond lengths around the vanadium centers are similar to those found in dioxidovanadium compounds with similar structures.[37] The bond lengths of the oxido ligands are slightly unequal, as V(1)═O(4) and V(2)═O(8) bonds are found to be 1.643(3) Å and 1.644(3) Å, whereas V(1)═O(3) and V(2)═O(7) are found to be 1.623(3) Å and 1.592(3) Å, respectively. This bond differentiation could be attributed to the fact that O(8) is also coordinated to two different sodium cations (Na(1) and Na(2)), bridging them together and also bridging both to the V(2) cation, whereas O(4) is singly bridging V(1) to Na(1). The atoms O(3) and O(7) are axially coordinated atoms, placed on top of the two tetragonal pyramids forming around the vanadium centers. In the basal plane, the Schiff base is coordinated to the vanadium center through five and six-membered chelate rings exhibiting bite angles 76.42° and 76.99° (for O(1)–V(1)–N(1) and O(5)–V(2)–N(2), respectively), and 81.54° and 81.67° (for O(2)–V(1)–N(1) and O(6)–V(2)–N(2), respectively). The six-membered coordination sphere around Na(1) also comprises two more bridging oxygen atoms from the phenolic moieties of two different $[\mathbf{L_3}]^{2-}$ ligands and two bound water molecules (O(9) and O(10)). The coordination geometry around Na(1) can be described as highly distorted trigonal prismatic, with O(1), O(4), O(10) and O(5), O(8), O(9) forming the trigonal bases. The second sodium cation, Na(2), was found to be five coordinate, with four bound water molecules (O(11), O(12), O(12)′ and (O13)) and O(8) as already described. The atoms Na(2), O(12), Na(2)' and O(12)′ form a parallelogram, with its center being the center of symmetry of the assembled octanuclear bimetallic complex.

A hydrogen-bonding network of twelve interactions is present in the crystal structure of the compound. All water molecules, coordinated or free, participate in these mainly intermolecular (eight out of the twelve) interactions, thereby creating molecular chains parallel to the *a* crystallographic axis and forming ultimately a 1D lattice (Fig. S3, ESI†).

Worth emphasizing in all of the above structures of derived materials **1–4** was the fact that: (a) all compounds involved mononuclear vanadium complexes, and (b) in all cases, the vanadium oxidation state was V(v). Confirmation of that contention, beyond X-ray crystallography, was achieved through EPR spectroscopy, with silent spectra observed in all cases (not shown), (c) the molecular stoichiometry of V(v) : ligand was 1 : 1, and (d) the deprotonation state of the ligand bound to vanadium was 2-. Moreover, quite interesting was the synthetic introduction of 4,4′-bipy in the coordination sphere of vanadium. Albeit quite successfully pursued in the case of compound **2** with ligand $[\mathbf{L_1}]^{2-}$ (a derivative of compound **1**), reflecting replacement of the bound methanol molecule in **1** by a 4,4′-bipy moiety, analogous reactions of vanadium with ligands $\mathbf{L_2H_2}$ and $\mathbf{L_3H_2}$ did not afford tractable crystalline materials (in the case of **3** and **4**) amenable to further physicochemical characterization. Quite distinct, however, was the correlation of the chemical reactivity of vanadium with the bulk nature of the ligand employed. In that respect, with the starting material in all cases being vanadium acetylacetonate (V(IV)), employment of 2-hydroxy-1-naphthaldehyde led to the isolation of crystalline material **4** bearing the $[VO_2]^+$ unit in the complex assembly. Inevitably, therefore, a characteristic difference between complexes **1–3** and **4** was the fact that the former species all contain V(v) in a $[VO]^{3+}$ core moiety, with the corresponding core

Table 2 Bond lengths [Å] and angles [deg] of $[VO(L_1)(CH_3O)(CH_3OH)]$ (**1**), $[VO(L_1)(CH_3O)](C_{10}H_8N_2)[VO(L_1)(CH_3O)]$ (**2**), $[VO(L_2)(CH_3O)(CH_3OH)]$ (**3**), and $[VO_2(L_3)Na(H_2O)_2VO_2(L_3)Na(H_2O)_3]_2{\cdot}H_2O$ (**4**)

1		2		3		4	
Distances (Å)							
V–O	1.588(3)	V(1)–O(1)	1.9064(17)	V(1)–O(1)	1.921(4)	V(1)–O(1)	1.906(3)
V–O(21)	1.769(3)	V(1)–O(2)	1.8602(15)	V(1)–O(2)	1.860(4)	V(1)–O(3)	1.623(3)
V–O(2)	1.860(2)	V(1)–O(3)	1.5975(17)	V(1)–O(3)	1.578(5)	V(1)–O(4)	1.644(3)
V–O(1)	1.939(2)	V(1)–O(5)	1.7760(16)	V(1)–O(4)	1.762(4)	V(1)–N(1)	2.189(3)
V–N	2.166(3)	V(1)–N(1)	2.1603(19)	V(1)–O(5)	2.392(4)	V(2)–O(5)	1.918(3)
V–O(22)	2.295(3)	V(1)–N(2)	2.4772(19)	V(1)–N(1)	2.158(5)	V(2)–O(6)	1.904(3)
				V(2)–O(6)	1.931(4)	V(2)–O(7)	1.592(3)
				V(2)–O(7)	1.850(4)	V(2)–O(8)	1.643(3)
				V(2)–O(8)	1.586(4)	V(2)–N(2)	2.160(3)
				V(2)–O(9)	1.759(4)	Na(1)–O(1)	2.275(3)
				V(2)–O(10)	2.388(4)	Na(1)–O(4)	2.537(3)
				V(2)–N(2)	2.147(5)	Na(1)–O(5)	2.347(3)
						Na(1)–O(8)	2.406(4)
						Na(1)–O(9)	2.333(4)
						Na(1)–O(10)	2.648(4)
						Na(2)–O(12)^{i}	2.442(4)
						Na(2)–O(8)	2.417(4)
						Na(2)–O(11)	2.393(4)
						Na(2)–O(12)	2.258(4)
						Na(2)–O(13)	2.143(5)
Angles (°)							
O–V–O(21)	102.10(13)°	O(1)–V(1)–O(2)	150.40(8)°	O(1)–V(1)–O(2)	153.3(2)°	O(1)–V(1)–O(2)	143.47(13)°
O–V–O(2)	98.15(13)°	O(1)–V(1)–O(3)	102.26(8)°	O(1)–V(1)–O(3)	101.4(2)°	O(1)–V(1)–O(3)	106.17(14)°
O(21)–V–O(2)	101.19(11)°	O(2)–V(1)–O(3)	99.89(8)°	O(2)–V(1)–O(3)	98.8(2)°	O(2)–V(1)–O(3)	105.99(13)°
O–V–O(1)	99.75(12)°	O(1)–V(1)–O(5)	93.14(8)°	O(1)–V(1)–O(4)	92.94(19)°	O(1)–V(1)–O(4)	91.25(13)°
O(21)–V–O(1)	92.88(11)°	O(2)–V(1)–O(5)	101.92(8)°	O(2)–V(1)–O(4)	99.5(2)°	O(2)–V(1)–O(4)	93.35(13)°
O(2)–V–O(1)	154.33(11)°	O(3)–V(1)–O(5)	100.43(9)°	O(3)–V(1)–O(4)	102.9(2)°	O(3)–V(1)–O(4)	110.56(15)°
O–V–N	92.60(12)°	O(1)–V(1)–N(1)	77.08(7)°	O(1)–V(1)–O(5)	79.06(17)°	O(1)–V(1)–N(1)	76.42(11)°
O(21)–V–N	163.65(12)°	O(2)–V(1)–N(1)	83.03(7)°	O(2)–V(1)–O(5)	78.73(18)°	O(2)–V(1)–N(1)	81.54(11)°
O(2)–V–N	83.53(11)°	O(3)–V(1)–N(1)	91.35(8)°	O(3)–V(1)–O(5)	172.7(2)°	O(3)–V(1)–N(1)	99.66(12)°
O(1)–V–N	77.43(11)°	O(5)–V(1)–N(1)	166.13(8)°	O(4)–V(1)–O(5)	84.30(19)°	O(4)–V(1)–N(1)	149.55(14)°
O–V–O(22)	173.06(12)°	O(1)–V(1)–N(2)	79.91(7)°	O(1)–V(1)–N(1)	76.90(19)°	O(5)–V(2)–O(6)	142.05(14)°
O(21)–V–O(22)	84.82(11)°	O(2)–V(1)–N(2)	77.65(7)°	O(2)–V(1)–N(1)	84.69(19)°	O(5)–V(2)–O(7)	106.86(16)°
O(2)–V–O(22)	79.68(11)°	O(3)–V(1)–N(2)	177.49(8)°	O(3)–V(1)–N(1)	93.2(2)°	O(6)–V(2)–O(7)	106.68(15)°
O(1)–V–O(22)	80.36(11)°	O(5)–V(1)–N(2)	80.62(8)°	O(4)–V(1)–N(1)	162.5(2)°	O(5)–V(2)–O(8)	91.06(14)°
N–V–O(22)	80.62(11)°	N(1)–V(1)–N(2)	87.91(7)°	O(5)–V(1)–N(1)	79.79(17)°	O(6)–V(2)–O(8)	94.34(14)°
				O(6)–V(2)–O(7)	153.97(19)°	O(7)–V(2)–O(8)	109.09(16)°
				O(6)–V(2)–O(8)	100.2(2)°	O(5)–V(2)–N(2)	76.99(11)°
				O(7)–V(2)–O(8)	99.5(2)°	O(6)–V(2)–N(2)	81.67(12)°
				O(6)–V(2)–O(9)	92.56(18)°	O(7)–V(2)–N(2)	97.29(14)°
				O(7)–V(2)–O(9)	99.60(18)°	O(8)–V(2)–N(2)	153.30(14)°
				O(8)–V(2)–O(9)	102.8(2)°		
				O(6)–V(2)–O(10)	80.01(15)°		
				O(7)–V(2)–O(10)	78.74(17)°		
				O(8)–V(2)–O(10)	174.10(19)°		
				O(9)–V(2)–O(10)	83.04(17)°		
				O(6)–V(2)–N(2)	77.69(17)°		
				O(7)–V(2)–N(2)	84.27(17)°		
				O(8)–V(2)–N(2)	93.28(19)°		
				O(9)–V(2)–N(2)	162.49(19)		

in **4** being $[VO_2]^+$ (*vide infra*). This observation should further be investigated to confirm or disprove the association of the bulky substituent with the specific core-containing vanadium center.

The composition of the coordination sphere of vanadium in all four materials was reflected in the nature of the ligand used in their synthesis and crystallization. In that sense, the first three complexes all had vanadium residing at the center of an octahedral assembly. A common feature in such an assembly involved: (a) the doubly deprotonated Schiff-base ligand occupying three sites in the equatorial plane, (b) the methoxido ligand occupying the fourth equatorial site, and (c) the solvent methanol moiety occupying the axial position trans to the oxido ligand in the $[VO]^{3+}$ group. As a consequence of such an arrangement, the protonated methanol moiety in the axial position seemed to be the one that could be replaced by another ligand. In that respect, methanol in complex **1** was easily replaced by 4,4′-bipyridine, with (a) methanol being the solvent of the synthesis reaction, and (b) retention of the coordination environment in **2** upon entry of 4,4′-bipyridine in the axial position of the coordination sphere of vanadium in **1**.

Employment of the bulkier 2-hydroxy-1-naphthaldehyde Schiff-base in the synthetic process led to the emergence of the $[VO_2]^+$-containing complex assembly, distinctly differentiating the nature of the complex emerging upon crystallization. Specifically,

the newly formulated coordination sphere of vanadium was composed of (a) the doubly deprotonated Schiff ligand occupying the three apices of the base of a tetragonal pyramid, (b) one of the oxido ligands occupying the fourth apex of the same tetragonal base of the pyramid, and (c) the second oxido ligand being at the apex of the pyramid, collectively giving rise to a pyramidal coordination environment for vanadium. Therefore, the employment of the bulky Schiff base in the synthesis differentiated the coordination environment of vanadium from octahedral in the first three species to tetragonal pyramidal in the fourth case. Quite interesting in that respect was also the observation that as a result of such a change in the synthetic process, the first three materials **1–3** involved molecular species bearing zero charge, whereas the fourth species was negatively charged (−1), thereby requiring the presence of a counter ion to achieve neutralization. Ostensibly, the presence of sodium and thus the inorganic base in the reaction mixture was involved in the formulation of the coordination sphere of vanadium, with employed organic bases failing to play that role (data not shown). Regardless, however, of the nature of the Schiff-base ligand employed in the synthesis, development of the reaction mixture under aerobic conditions was the most noted signature of the investigated reactivity, initially involving V(IV) and ultimately affording V(V)-containing species. On an equal footing, exploration of the exclusion of oxygen from the reactivity mentioned is a factor warranting investigation, currently probed into in our lab.

2.2.2 FT-IR spectroscopy. The infrared spectra of **1–4** show active ν(OH) and ν(C=N) vibrations at 3380 cm^{-1} and 1605 cm^{-1} for **1**, 3441 cm^{-1} and 1638 cm^{-1} for **2**, 3430 cm^{-1} and 1617 cm^{-1} for **3**, and 3443 cm^{-1} and 1606 cm^{-1} for **4**, respectively. Binding of the azomethine nitrogen is revealed by lowering of the resonance frequency (10–23 cm^{-1}). The characteristic ν(V=O) stretch appears as a medium-strong band at 967 cm^{-1} for **1**, 949 cm^{-1} for **2**, 982 cm^{-1} for **3**, and 962 cm^{-1} for **4**, respectively, which is in line with the literature.[38,39] The absorption bands at 1602 cm^{-1} and 1039 cm^{-1} for **2** are indicative of the ν(C–N) of the 4,4′-bipy moiety. The individual characteristic spectral features observed are analogous to those previously observed and reported.[38,39]

2.2.3 ESI-MS spectrometry. ESI-MS spectrometry was employed under optimal experimental conditions to probe the behavior of the title compounds in solution. The ESI-MS spectrum of **1** in methanol reveals the presence of fragments m/z = 355.02 with z = 1, reflecting species $[VO_2(L_1)(CH_3O)]^+$ (Fig. S4, ESI†). The spectrum of **2** in water reveals the presence of fragments m/z = 265.12 with z = 1 reflecting species $[(L_1) + 1](Na^+)$, and m/z = 324.01 with z = 1, reflecting species $[VO_2(L_1)]$, thereby attesting to the vanadium:ligand stoichiometry of 1 : 1 (Fig. S5, ESI†). Dissociation of 4,4′-bipyridine from the compound molecule was attested to in the positive mode of ionization, whereby the presence of the 4,4′-bipyridinium ion $[C_{10}H_9N_2]^+$ was observed, with m/z = 157.07 and z = 1. In the case of compound **3**, the spectrum suggests the presence of m/z = 293.99 with z = 1 species, thus reflecting the $[VO_2(L_2)]$ moiety (Fig. S6, ESI†), with the complex retaining the metal : ligand stoichiometry of 1 : 1. The spectrum of compound **4** in water shows the presence of m/z = 344.01 with z = 1 species, reflecting the $[VO_2(L_3)]$ moiety (Fig. S7, ESI†), with the assembly retaining its metal : ligand stoichiometry of 1 : 1. The collective spectra provide ample clarification on the nature of species emerging upon dissolution of the original crystalline materials in aqueous media, thereby lending credence to the ensuing biological studies.

2.2.4 UV-Vis spectroscopy. The electronic spectra of **1–4** (Fig. S8, ESI†) were obtained in MeOH at a concentration of 10^{-4} M, at room temperature. In all cases, the spectra show two intense bands and one relatively weak band in the 227–467 nm region. The intense band at 227 nm (ε = 3880 mol^{-1} cm^{-1}) for **1**, 231 nm (ε = 4020 mol^{-1} cm^{-1}) for **2**, 231 nm (ε = 4010 mol^{-1} cm^{-1}) for **3**, and 231 nm (ε = 4020 mol^{-1} cm^{-1}) for **4**, respectively, can be assigned to the $\pi \rightarrow \pi^*$ transitions of the aromatic rings, with the less intense band at 371 nm (ε = 1150 mol^{-1} cm^{-1}) for **1**, 370 nm (ε = 1190 mol^{-1} cm^{-1}) for **2**, 372 nm (ε = 1540 mol^{-1} cm^{-1}) for **3**, and 371 nm (ε = 1580 mol^{-1} cm^{-1}) for **4**, respectively, attributed to the $\pi \rightarrow \pi^*$ and $n \rightarrow \pi^*$ transitions of the C=N moiety.[40] The very intense band at 431 nm (ε = 2330 mol^{-1} cm^{-1}) for **1**, 421 nm (ε = 2330 mol^{-1} cm^{-1}) for **2**, 467 nm (ε = 6670 mol^{-1} cm^{-1}) for **3**, and 445 nm (ε = 5110 mol^{-1} cm^{-1}) for **4**, respectively, can be correlated with the O(p) → V(d) ligand-to-metal charge transfer (LMCT) transition, thereby providing strong evidence that $[VO(OR)]^{2+}$ is coordinated to the phenolato oxygen atom of the ligand.[41] Here, too, the electronic spectral features were analogous to those previously observed and support the notion of complex species present in solution.[40]

2.2.5 Thermal studies. The thermal decomposition of compounds **1–4** was studied by TGA under aerobic conditions (Fig. S9, ESI†). Compound **1** is thermally stable up to 45 °C. From that point on, a fairly broad heat process points to the release of the coordinated methanol molecule of **1** between 45 °C and 329 °C. In fact, a 8.4% drop in weight, from the start of the thermal treatment until 329 °C, is consistent with the release of the methoxy molecule in the coordination sphere of vanadium, consistent with the theoretically expected value of 8.6%. Between 329 °C and 442 °C, a further weight loss is observed, in line with the decomposition of the organic structure of the molecule. No clear plateaus are reached in this temperature range, suggesting that the formed products are unstable and decompose further. A plateau in the decomposition of **1** is reached at 442 °C, with no further loss up to 550 °C, in line with the thesis that the product at that temperature and beyond (550 °C) is V_2O_5. The total weight loss of ∼76.0% is in agreement with the theoretical value of ∼75.5%, according to the following equation:

$$4[VO(C_{14}H_{11}NO_3)(CH_3O)(CH_3OH)] + 79O_2 \rightarrow 2V_2O_5 + 64CO_2 + 4NO_2 + 36H_2O$$

Compound **2** is thermally stable up to 167 °C. Between 167 °C and 513 °C, a weight loss is observed, in line with the decomposition of the organic structure of the molecule. No clear plateaus are reached in this temperature range, suggesting that the formed products are unstable and decompose further. A plateau in the decomposition of **2** is reached at 513 °C, with no further loss up to 550 °C, in line with the thesis that the product

at that temperature and beyond (550 °C) is V_2O_5. The total weight loss of ~78.7% is in agreement with the theoretical value of ~78.2%, according to the following equation:

$$2\{[VO(C_{14}H_{11}NO_3)(CH_3O)][(C_{10}H_8N_2)[VO(C_{14}H_{11}NO_3)(CH_3O)]\} + 101O_2 \rightarrow 2V_2O_5 + 80CO_2 + 8NO_2 + 36H_2O$$

Compound **3** is thermally stable up to 244 °C. Between 244 °C and 513 °C, a weight loss is observed, in line with the decomposition of the organic structure of the molecule. No clear plateaus are reached in this temperature range, suggesting that the resultant products undergo further decomposition. A plateau in the decomposition of **3** is reached at 542 °C, with no further loss up to 550 °C, in line with the product at that temperature and beyond (550 °C) being V_2O_5. The total weight loss of ~73.0% is in agreement with the theoretical value of ~73.4%, according to the following equation:

$$4[VO(C_{13}H_9NO_2)(CH_3O)(CH_3OH)] + 75O_2 \rightarrow 2V_2O_5 + 60CO_2 + 4NO_2 + 32H_2O$$

Compound **4** is thermally stable up to 269 °C. Between 269 °C and 504 °C, a weight loss is observed, in line with the decomposition of the organic structure of the molecule. No clear plateaus are reached in this temperature range, suggesting that the resultant products undergo further decomposition. A plateau in the decomposition of **3** is reached at 504 °C, with no further loss up to 550 °C, in line with the product at that temperature and beyond (550 °C) being $NaVO_3$. The total weight loss of ~71.0% is in agreement with the theoretical value of ~70.7%, according to the following equation:

$$\{[VO_2(C_{17}H_{11}NO_2)]_2[Na_2(H_2O)_5]\}_2{\cdot}H_2O + 81O_2 \rightarrow 4NaVO_3 + 68CO_2 + 4NO_2 + 33H_2O$$

The described tentative assignments are consistent with previously reported results on thermogravimetric analysis.[37,42]

The collective physicochemical characterization of all four species (elemental analysis, FT-IR, EPR, UV-Visible spectroscopy, and X-ray crystallography) was consistent with the formulation unraveled by the structural characterization of the materials. Further investigation of the solution behavior of the four complexes through ESI-MS spectrometry led to the formulation of their profile in solution, thereby lending credence to their employment in the subsequent biological studies.

2.3 Cytotoxicity studies

2.3.1 Ligand toxicity in 3T3-L1 pre-adipocytes. To investigate the potential cytotoxic effects of the organic ligands-substrates L_iH_2 (i = 1–3) on 3T3-L1 pre-adipocytes, cells were treated with 1, 10, 100, 200 μM of $\mathbf{L_1H_2}$, $\mathbf{L_2H_2}$, and $\mathbf{L_3H_2}$, respectively, for 24 h (Fig. S10A–C, ESI†). The results show that all three ligands do not affect cell survival under the employed experimental conditions. L_1H projects a slight concentration-dependent cytotoxic profile ($p > 0.05$). In particular, cell survival amounts to 112.1% at 1 μM, 108.6% at 10 μM, 94.7% at 100 μM, and ~90% at 200 μM ($p < 0.05$) in the presence of $\mathbf{L_1H_2}$. $\mathbf{L_2H_2}$ and $\mathbf{L_3H_2}$ are completely atoxic at all concentrations tested ($p > 0.05$).

2.3.2 V(v) compound toxicity in 3T3-L1 pre-adipocytes for 24 h. To examine whether the newly-synthesized V(v) compounds (**1–4**) affect cell survival rates, 3T3-L1 pre-adipocytes were treated with 1, 10, 50, and 100 μM of the title compounds for 24 h. Fig. 5A–D shows that all four compounds affect cell survival in a concentration-dependent fashion under the employed experimental conditions. More specifically, cell survival, in the presence of **1**, stands at 106.7% at 1 μM, 99.1% at 10 μM, 96.0% at 50 μM, and 71.3% at 100 μM ($p > 0.05$). In the case of **2**, cell survival stands at 96.5% at 1 μM, 95.1% at 10 μM, 74.3% at 50 μM ($p > 0.05$), and 28.2% at 100 μM ($p < 0.001$). Similarly, cell survival stands at 79.4%, 71.6%, 40.2% and 6.4% at 1, 10, 50, and 100 μM, respectively, following exposure to **3**, and 98.3%, 80.7, 64.8, and 51.6% in the case of **4**, and for the same concentration range.

2.3.3 V(v) compound toxicity in 3T3-L1 pre-adipocytes for 48 h. Similarly, cell survival was also assessed in the same concentration range (1–100 μM), following treatment with **1–4** for 48 h, since cells, during induction of the differentiation process, are exposed to the title compounds for more than 24 h. The results in Fig. 6A–D show that the tested compounds affect cell survival in a concentration-dependent manner. It should be mentioned, however, that for longer incubation times (48 h), V(v)-compounds exerted a proliferative effect in most cases. Cell viability stands at 179.6%, 132.0%, 103.6% and 101.2% following treatment with **1** at 1, 10, 50, and 100 μM, respectively. In the case of **2**, cell viability stands at 96.9%, 140.0%, 147.5%, and 42.1% for the same concentration range. Compound **3** was completely atoxic at low concentrations (103.1% and 95.4% at 1 and 10 μM, respectively), whereas at higher concentrations cell survival was significantly reduced (5.2% and 0.5% at 50 μM and 100 μM, respectively). Compound **4** projected a cytotoxic behavior similar to **3**. More specifically, cell survival amounts to 102.8%, 110.7%, 52.4%, and 3.7% in the range 1–100 μM compared to the control (untreated cells).

In previous studies,[37] it had been shown that V(v), in the form of KVO_3, affects 3T3-L1 cell survival in a concentration-dependent manner for concentrations higher than 1 μM. To this end, it becomes evident that ligation alters the cytotoxic behavior of the complex vanadoforms. More specifically, in the present work, ligation enhances the bioavailability of the title compounds and limits the cytotoxic profile under the employed experimental conditions. Taken together, all four compounds can further be used to examine the potential insulin-mimetic properties towards adipogenesis.

2.3.4 Cell migration–cell morphology. Since the specific cell line exerts cell migration properties, in an effort to investigate the potential effects of the title compounds on the endogenous cell migration of 3T3-L1 pre-adipocytes, an *in vitro* scratch assay was performed. The physiological migrating activity of cells, grown in the presence of only DMEM, was considered as control. Cells were treated with 10 μM (a concentration with mild toxicity for all compounds) of each V(v)-compound (**1–4**) for 24 and 48 h, respectively (10× 5× magnification). As shown in Fig. 7, cells exhibited full inhibition of cell migration in the case of **1** and **4**,

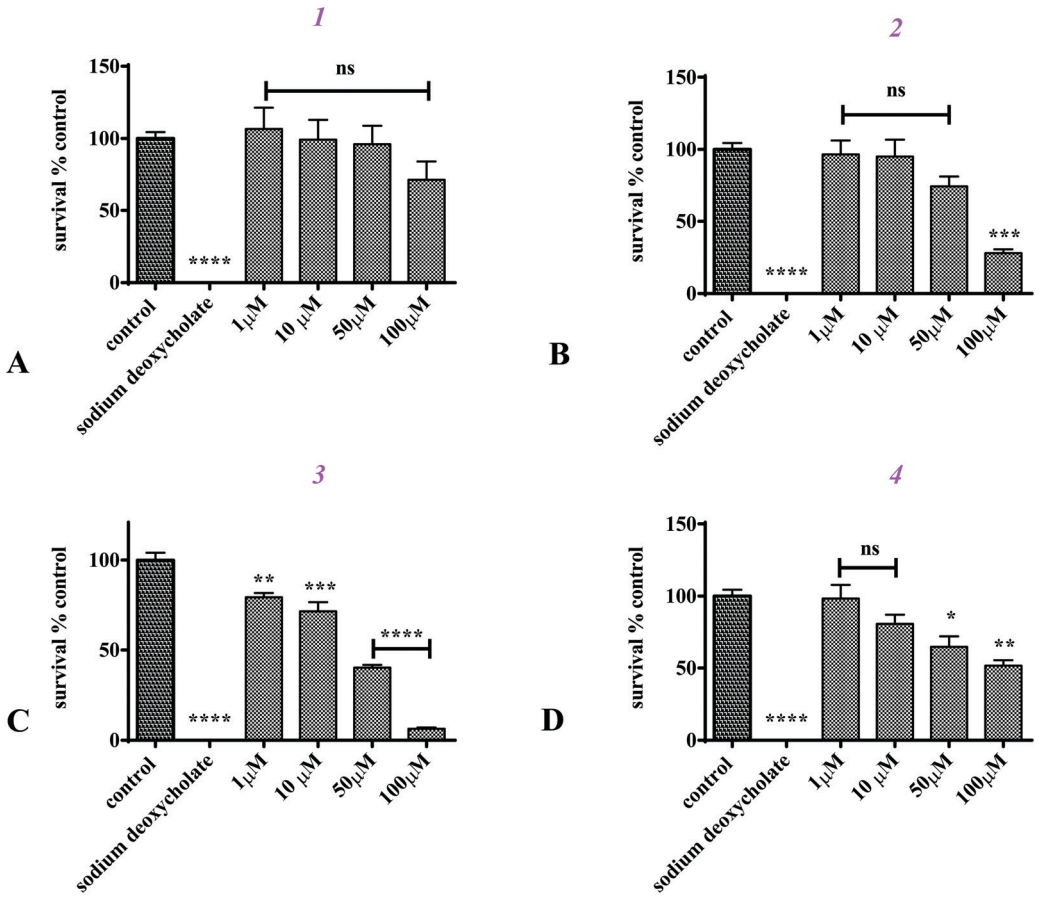

Fig. 5 Percent of cell survival in 3T3-L1 pre-adipocytes following treatment with various concentrations (1–100 μM) of **1** (**A**), **2** (**B**), **3** (**C**), and **4** (**D**) for 24 h. Sodium deoxycholate has been used as a positive control. Values represent the mean value of several (n = 3) independent experiments. Vertical bars represent SEMs. *$p < 0.05$ (significant), **$p < 0.01$ (highly significant), ***$p < 0.001$ (extremely significant) and ****$p \leq 0.0001$ (extremely significant) or non-significant ($p > 0.05$).

whereas cell migration was slightly inhibited in the presence of **2** and **3** after 24 h compared to control. Similar results were also obtained following treatment for 48 h (data not shown).

2.4 Insulin-mimetic/enhancing studies

2.4.1 V(v)-compound oil red O staining results. In an effort to investigate the adipogenic and thus insulin mimetic and/or enhancing activity of the newly synthesized materials, the title compounds were employed to induce cell differentiation of 3T3-L1 fibroblasts into mature adipocytes, following a standard differentiation protocol. Oil red O staining was performed on the 8th day of the differentiation process to examine the lipid content of mature adipocytes differentiated in the presence of **1–4**. As assessed through staining, **1** induced differentiation of pre-adipocytes into mature adipocytes at all concentrations tested (1 and 20 μM), compared to control (untreated cells, Fig. 8A), whereas no synergistic or inhibiting effect was observed when cells were treated in combination with insulin (20 μM of **1** with insulin) (Fig. 8C–E) compared to positive control (insulin) (Fig. 8B). In the case of **2**, cell differentiation was achieved when the compound was used alone in a slight concentration-dependent manner (Fig. 8F and G). The effect was clearly enhanced when **2** was used in combination with insulin compared to control (Fig. 8H), but it was significantly lower compared to positive control. In an analogous fashion, **3** and **4** were also employed to induce cell differentiation of 3T3-L1 fibroblasts into mature adipocytes either by fully replacing insulin or in combination with it. In both cases, the effect was comparable to the differentiation effect induced by insulin (Fig. 8I–N). Oil red O staining is a qualitative assay, assessing the potential adipogenic activity of various agents. Thus, no quantitative results can be obtained. However, the assay can be used to investigate the synergistic/enhancing or inhibiting effect of such agents. In the present study, all compounds tested induced adipogenesis either alone or in combination with insulin. The concentrations used were selected based on the cytotoxicity results for 24 and 48 h. To further validate and quantitatively evaluate the adipogenic potential of **1–4**, the relative mRNA expression of closely linked biomarkers (PPAR-γ, GLUT4, ADIPOQ, INS-R, and RETN) was also investigated.

2.4.2 Relative mRNA expression of related biomarkers (PPAR-γ, GLUT4, ADIPOQ, INS-R, and RETN). On the 8th day of the differentiation process, total mRNA was extracted and RT-PCR was run to examine the relative mRNA expression of selected molecular targets. In that sense, the relative mRNA concentration was determined for PPAR-γ, GLUT4, ADIPOQ,

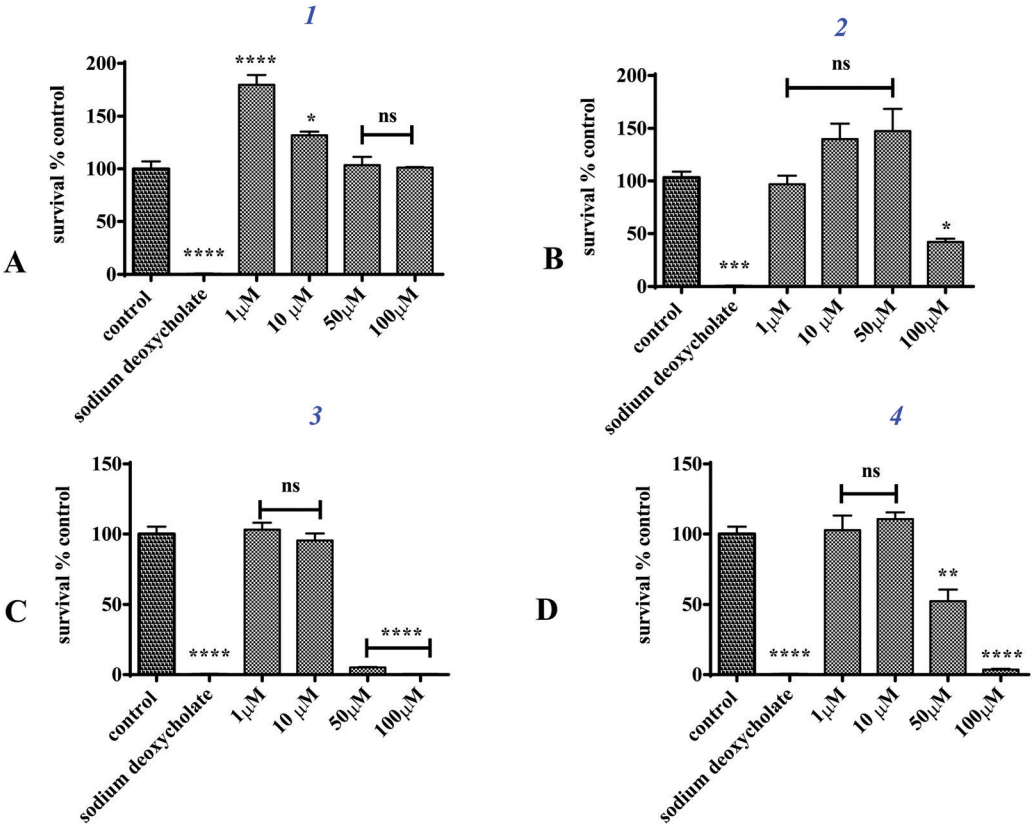

Fig. 6 Percent of cell survival in 3T3-L1 pre-adipocytes following treatment with various concentrations (1–100 μM) of **1** (**A**), **2** (**B**), **3** (**C**), and **4** (**D**) for 48 h. Sodium deoxycholate has been used as a positive control. Values represent the mean value of several (n = 3) independent experiments. Vertical bars represent SEMs. *$p < 0.05$ (significant), **$p < 0.01$ (highly significant), ***$p < 0.001$ (extremely significant) and ****$p \leq 0.0001$ (extremely significant) or non-significant ($p > 0.05$).

INS-R, and RETN. Initially, the expression of PPAR-γ was investigated, which serves as a key transcription factor during adipogenesis, influencing more than 2000 genes involved in the specific process.[43,44] Cells were treated with **1–4** at 1 μM and 20 μM or in combination with insulin (20 μM with insulin). Again, untreated cells were considered as negative control of the assay, whereas insulin alone (standard differentiation protocol) as the positive control. Insulin alone projected a 4-fold increase (Fig. 9). In the case of **1**, PPAR-γ projects a 10.5 fold increase at 1 μM and 8.5 fold increase at 20 μM. When **1** is used in combination with insulin, PPAR-γ is slightly expressed (∼1.9 fold increase), thus indicating a potential inhibiting effect toward insulin action under the employed experimental conditions for this gene (Fig. 9A). By the same token, in the case of **2**, PPAR-γ projected a 7-fold increase at 1 μM and 1.1-fold increase at 20 μM. When **2** was used in combination with insulin, the relative mRNA expression of PPAR-γ was almost the same as that of insulin alone (∼3.9) (Fig. 9B). Given the fact that **2** has almost no effect, when used alone at 20 μM and the expression levels in combination with insulin are equal to that of insulin alone, the obtained results indicate that the observed effect is due to insulin and **2** has no effect (either enhancing or inhibiting) on insulin action (Fig. 9B). In the case of **3**, the expression of PPAR-γ is 1.2 and 2 at 1 μM and 20 μM, respectively, whereas when **3** is used in combination with insulin the fold increase is 6.3. The results indicate a slight concentration-dependent effect and a synergistic/enhancing effect on insulin compared to positive control (Fig. 9C). When cells were differentiated in the presence of **4**, relative mRNA expression of PPAR-γ was 2.6 and 4.2 at 1 μM and 20 μM, respectively. When cells were treated with **4** in combination with insulin, relative mRNA expression was 1.8, indicating a potential inhibiting effect toward insulin action under the employed experimental conditions considering this gene (Fig. 9D).

Similarly, the relative mRNA expression of GLUT4 was also determined, in view of the fact that the specific gene is only expressed in mature adipocytes, serving as a biomarker of successful differentiation. In the case of **1**, relative mRNA expression exhibited a 6.8- and 6.6-fold increase at 1 μM and 20 μM, respectively, compared to control, whereas in combination with insulin, **1** projected a 4.8-fold increase (Fig. 10A). The results indicate that there is no significant difference between the two concentrations employed. Moreover, **1** has no effect on insulin action compared to positive control (∼5 fold increase). In the case of **2**, the relative mRNA expression of GLUT4 is 2.4 at 1 μM and 1.8 at 20 μM (Fig. 10B). When **2** is used in combination with insulin, the fold increase is ∼6, indicating a slight insulin-enhancing effect. In the case of **3**, the relative mRNA expression is 3.8 at 1 μM, 15.7 at 20 μM, and 3.7 when **3** is used in combination with insulin (Fig. 10C). The results indicate a concentration-dependent

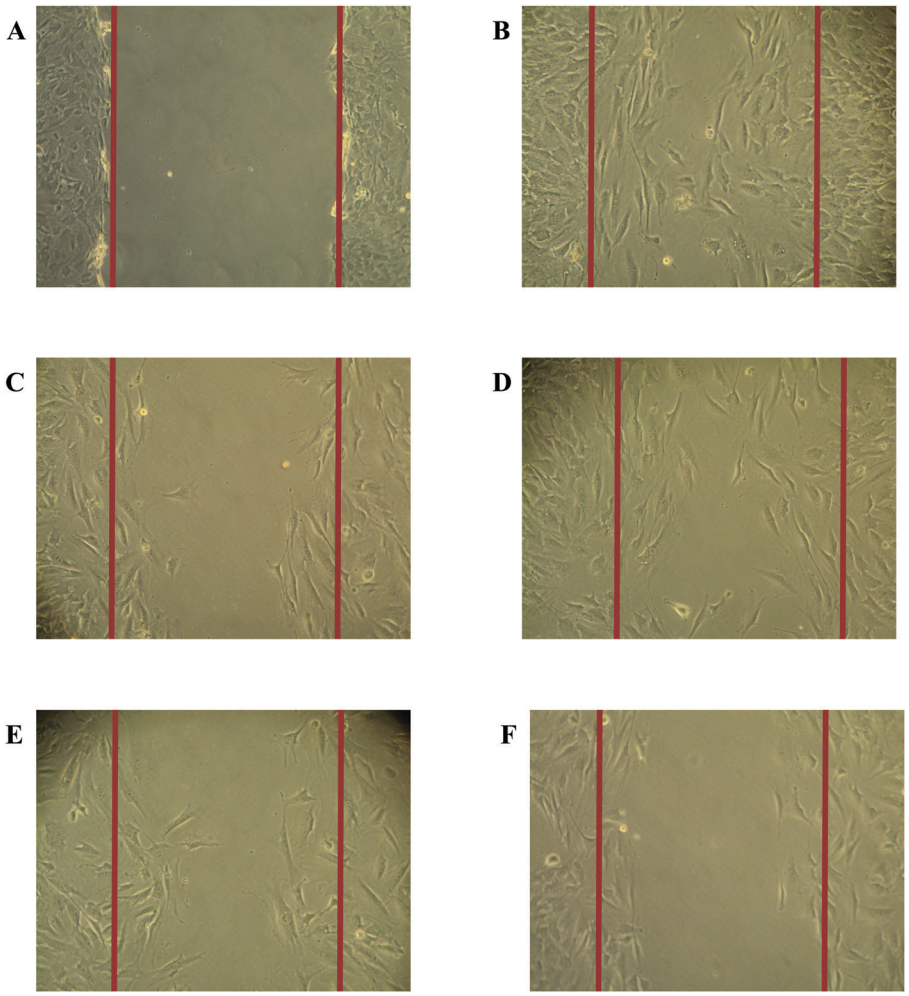

Fig. 7 Cell migration of 3T3-L1 (**A**) control (t = 0), (**B**) control after 24 h, (**C**) cells treated with 10 μM of **1**, (**D**) **2**, (**E**) **3**, and (**F**) **4** using an *in vitro* standard scratch assay.

effect when **3** is used alone, yet interestingly, **3** exhibits an inhibiting/competitive effect towards insulin action. Similarly, when cells are differentiated in the presence of **4**, the mRNA expression of GLUT4 is 4.5 at 1 μM, 9.7 at 20 μM, and ~5 when **4** is used in combination with insulin (Fig. 10D).

It is well-established that adipose tissue is capable of secreting several adipocytokines closely related to the metabolic status among others.[45] Besides GLUT4, adiponectin (ADIPQ) also serves as a valid biomarker of successful adipogenesis.[46] In that sense, the relative mRNA expression of adiponectin was examined at the end of the differentiation process. Again, untreated cells were considered as control and differentiation with insulin alone as the positive control (7.6-fold increase) (Fig. 11). When cells are differentiated in the presence of **1**, the relative expression is 10.3 and ~9 at 1 and 20 μM, respectively. When cells are differentiated in combination of **1** and insulin, the expression of ADIPOQ is 18.7, indicating an insulin enhancing effect of **1** toward insulin (Fig. 11A). In the case of **2**, the expression pattern is concentration-dependent (~3 and 8.7 at 1 and 20 μM, respectively), whereas combination of **2** and insulin shows an 8.5-fold increase (equal to that of cells treated only with 20 μM of **2**). The specific result indicates a potential antagonism between **2** and insulin rather than a slight synergistic effect (Fig. 11B). In an analogous fashion, **3** and **4** exhibit a concentration-dependent expression of ADIPOQ (4.8 and 6.6 for **3** and 4.9 and 7.3 for **4** at 1 and 20 μM, respectively) (Fig. 11C and D). The combination of **3** and insulin exhibits a 6.9-fold increase, whereas in the case of **4** the fold increase is 5.6. It is worth pointing out that only **1** projects higher expression levels in all concentrations/cases used.

Furthermore, expression levels for resistin were also investigated (Fig. 12). Resistin, also known as the adipose tissue-specific secretory factor (ADSF) or C/EBP–epsilon-regulated myeloid-specific secreted cysteine-rich protein (XCP1), is a cysteine-rich adipose-derived peptide hormone, which in humans is encoded by the RETN gene. Although the role of resistin in obesity is still questionable, it is well-established that the specific adipokine is secreted by white adipose tissue and could be used as a biomarker of successful adipogenesis. The mature adipocytes differentiated in the presence of insulin project a 3-fold increase compared to control (untreated cells) (Fig. 12). In the case of **1**, the expression of resistin is 6.6 and 2.6, when cells are differentiated with 1 and

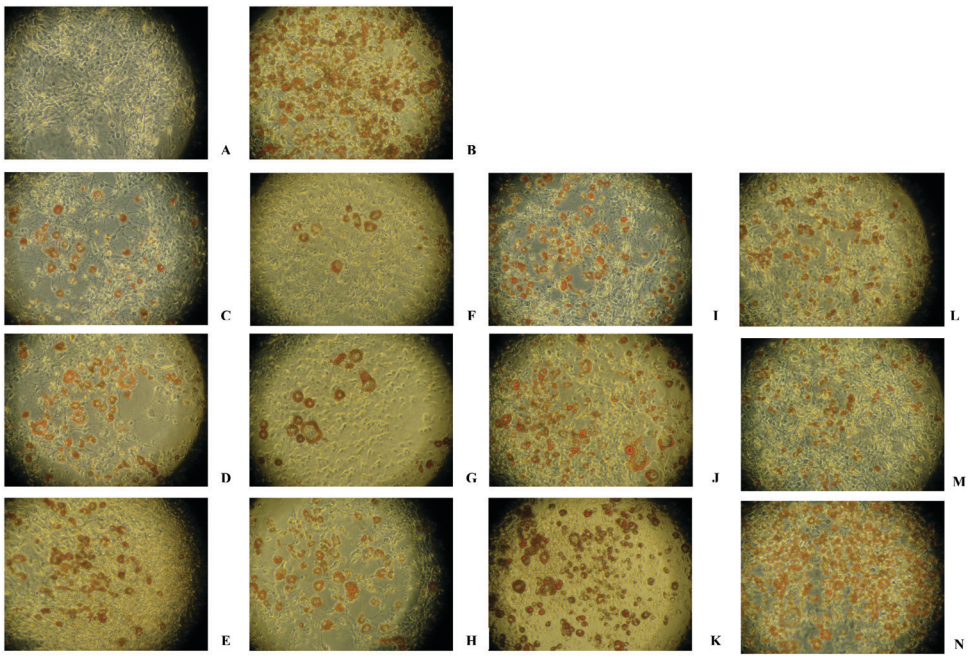

Fig. 8 Representative micrographs of 3T3-L1 pre-adipocyte differentiation, as assessed by oil red O staining. (**A**) Untreated cells, (**B**) mature adipocytes differentiated in the presence of insulin (10 ng mL^{-1}), mature adipocytes differentiated in the presence of 1, 20 μM, and 20 μM, in combination with insulin of **1** (**C**–**E**), **2** (**F**–**H**), **3** (**I**–**K**), and **4** (**L**–**N**).

20 μM, respectively. When **1** is used in combination with insulin, the relative expression is 5.2 (Fig. 12A). In the case of **2**, the relative expression of resistin is 2.6 and 4.0 at 1 and 20 μM, respectively, whereas when cells are treated with **2** in combination with insulin the relative expression level is 4.8 (Fig. 12B). Similarly, in the case of **3**, resistin projects a 5.4 and 4.1-fold increase at 1 and 20 μM, respectively, and 4.2 when cells are treated in combination of **3** and insulin (Fig. 12C). Finally, in the case of **4**, the expression levels are ∼4 and 6.6 when cells are treated with 1 and 20 μM, respectively, and 7.6 when cells are treated in combination with insulin, thus indicating a synergistic effect of **4** toward insulin (Fig. 12D). The relative mRNA expression of the insulin receptor (INS-R) was also assessed on the 8th day of the differentiation process, to examine any potential variation of the expression pattern between premature and mature adipocytes.[47] The results show that there is no significant fold increase expression (a) between pre-mature and mature adipocytes (pre-adipocytes *vs.* treated ones with insulin), and (b) when cells are treated with **1**–**4** or in combination with insulin (data not shown).

Inevitably, the complex forms of vanadium developed over the years have involved parameters including its oxidation state, ligand nature, charge, and hydrophilicity, among others. As a result of such features having been taken into consideration, the synthesized vanadium complexes have exhibited variable physicochemical properties linked to their ultimate insulin mimetic activity. In view of the fact that such biological activity applies to different phases of the cellular functions leading to glucose uptake, the present investigation revolved around the design of the vanadium coordination environment that could influence adipocyte differentiation processes intimately linked to insulin mimesis. To that end, the choice of ligands formulating vanadium coordination was driven toward appropriately configured Schiff bases and the oxidation state of vanadium being V(v). The latter oxidation state is one of the biologically relevant oxidation states of vanadium in biological fluids. The Schiff base series relied on a common 2-aminophenol moiety attached to an *o*-vanillin core, with the latter structure sequentially modified through removal of the methoxy substituent on the aromatic ring and the concurrent derivatization of the core through annexation of yet another aromatic substituent, thereby enhancing the bulk and hydrophobicity of the Schiff base. In almost all cases investigated so far, the expression pattern of GLUT4 follows the PPAR-γ expression pattern. This observation is consistently in line with the literature.[48]

3. Experimental section

3.1 Materials and methods

All experiments were carried out under aerobic conditions. The structures of the ligands used are listed in Scheme 1. The following starting materials were purchased from commercial sources (Sigma, Fluka) and were used without further purification: 2-aminophenol, *o*-vanillin, 2-hydroxy-1-naphthaldehyde, salicylaldehyde, 4,4′-bipyridine (4,4′-bipy) and vanadyl acetylacetonate ($VO(C_5H_7O_2)_2$); solvents: ultrapure water, methanol, and diethyl ether. The isolated complexes, dried under vacuum at room temperature, are air-stable.

3.2 Physical measurements

FT-Infrared spectra were recorded on a PerkinElmer 1760X FT-infrared spectrometer. A ThermoFinnigan Flash EA 1112

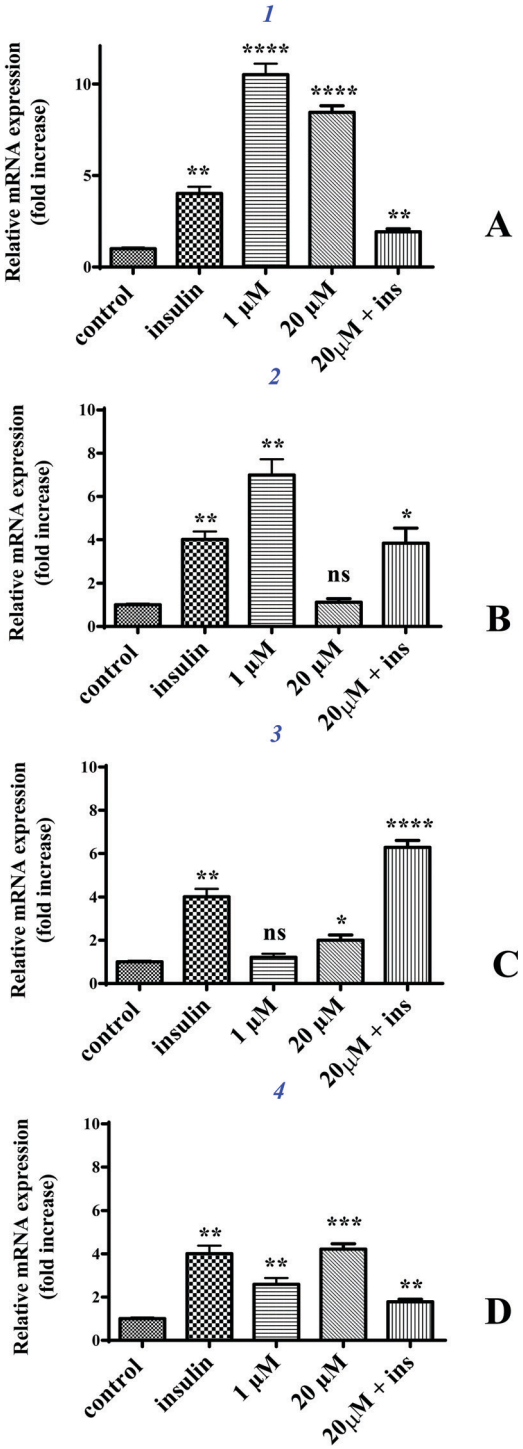

Fig. 9 Relative concentration of mRNA expression for PPAR-γ in mature adipocytes treated with insulin or **1** (**A**), **2** (**B**), **3** (**C**), and **4** (**D**) compared to pre-adipocytes on the 8th day of the differentiation process. Values represent the mean value of several (n = 3) independent experiments. Vertical bars represent SEMs; non-significant ($p > 0.05$); *: $p < 0.05$; **: $p < 0.01$; ***: $p < 0.001$ *vs.* control.

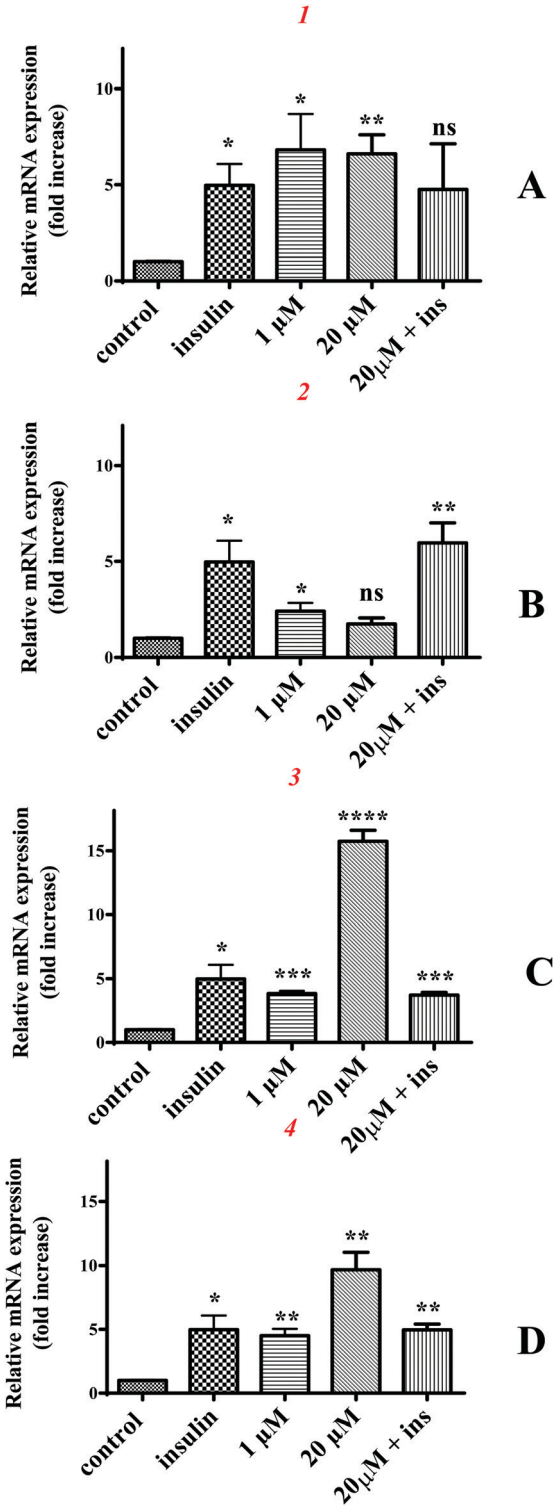

Fig. 10 Relative concentration of mRNA expression for GLUT4 in mature adipocytes treated with insulin or **1** (**A**), **2** (**B**), **3** (**C**), and **4** (**D**) compared to pre-adipocytes on the 8th day of the differentiation process. Values represent the mean value of several (n = 3) independent experiments. Vertical bars represent SEMs; non-significant ($p > 0.05$); *: $p < 0.05$; **: $p < 0.01$; ***: $p < 0.001$ *vs.* control.

CHNS elemental analyser was used for the simultaneous determination of carbon, hydrogen, and nitrogen (%). The analyser operation is based on the dynamic flash combustion of the sample (at 1800 °C) followed by reduction, trapping, complete GC separation and detection of the products. The instrument is

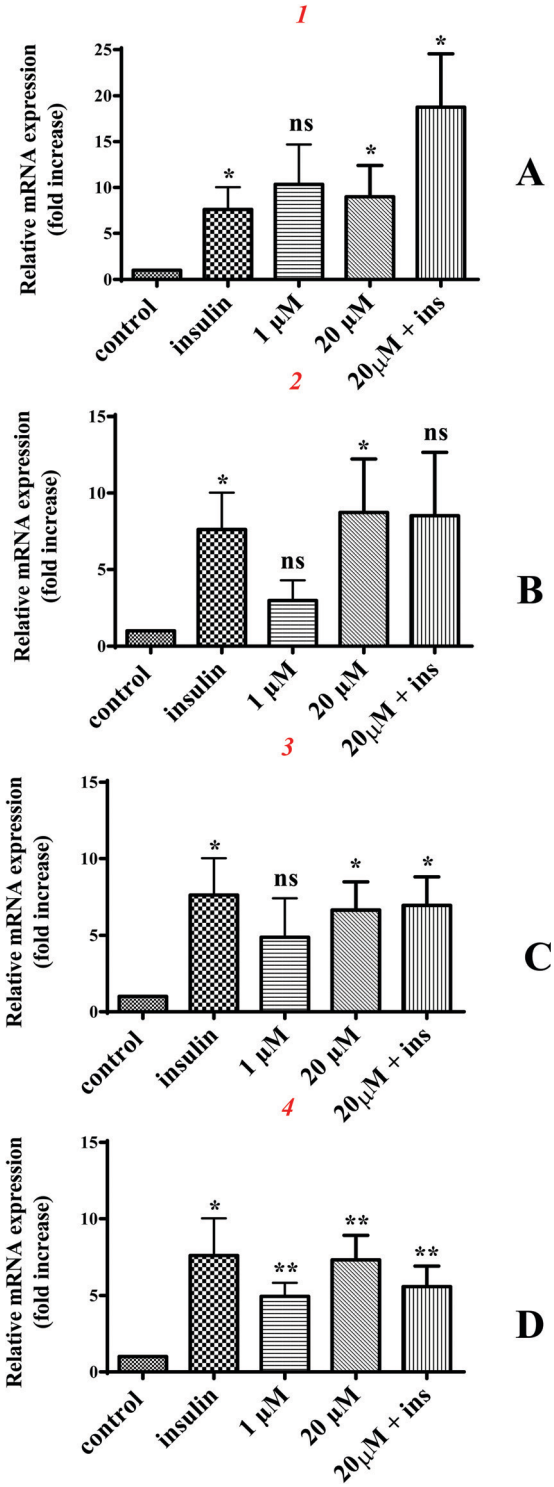

Fig. 11 Relative concentration of mRNA expression for ADIPOQ in mature adipocytes treated with insulin or **1** (**A**), **2** (**B**), **3** (**C**), and **4** (**D**) compared to pre-adipocytes on the 8th day of the differentiation process. Values represent the mean value of several (n = 3) independent experiments. Vertical bars represent SEMs; non-significant ($p > 0.05$); *: $p < 0.05$; **: $p < 0.01$; ***: $p < 0.001$ *vs.* control.

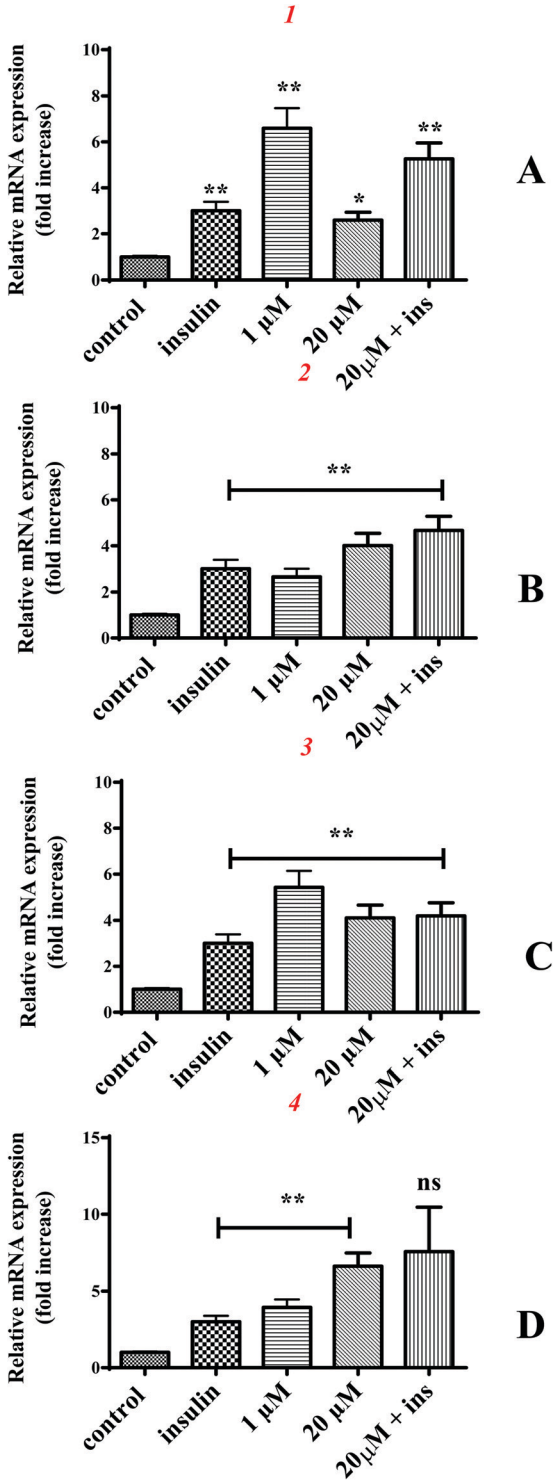

Fig. 12 Relative concentration of mRNA expression for RETN in mature adipocytes treated with insulin or **1** (**A**), **2** (**B**), **3** (**C**), and **4** (**D**) compared to pre-adipocytes on the 8th day of the differentiation process. Values represent the mean value of several (n = 3) independent experiments. Vertical bars represent SEMs; non-significant ($p > 0.05$); *: $p < 0.05$; **: $p < 0.01$; ***: $p < 0.001$ *vs.* control.

(a) fully automated and controlled by PC *via* the Eager 300 dedicated software, and (b) capable of handling solid, liquid or gaseous substances. Electron paramagnetic resonance (EPR) spectra were recorded at liquid N_2 temperature (77 K) on a

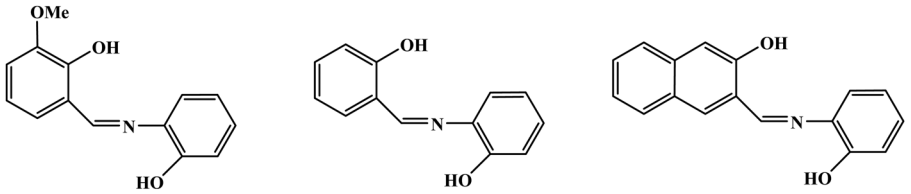

L_1H_2 L_2H_2 L_3H_2

Scheme 1 Schematic representation of the ligands (L_1H_2, L_2H_2, L_3H_2) used in this study.

Bruker ER200D spectrometer, equipped with an Agilent 5310A frequency counter. The spectrometer runs under home-made software based on LabView. Typically, adequate signal-to-noise ratio was obtained after 3–5 scans. EPR samples were prepared in 5 mm suprasil (Willmad Co.) quartz tubes with no further treatment.

3.3 UV-Visible measurements

UV-Visible (UV-Vis) measurements were carried out on a Hitachi U-2001 spectrophotometer, in the range from 190 to 1000 nm.

3.4 Thermal studies

A PerkinElmer, Pyris 1, system was used to run the simultaneous Thermogravimetric Analysis (TGA) experiments. The instrument mass precision is 1 μg. About 2–5 mg of compounds **1–4** was placed in an open alumina sample pan for each experiment. High purity air was used at a constant flow rate of 30 mL min^{-1}, depending on the conditions required for running the experiments. During the experiments, the sample weight loss and rate of weight loss were recorded continuously under dynamic conditions, as a function of time or temperature, in the range 30–550 °C. Prior to activating the heating routine program, the entire system was purged with the appropriate gas for 10 min, at a rate of 30 mL min^{-1}, to ensure that the desired environment had been established.

3.5 ESI-MS measurements

The electron spray ionization mass spectrum was obtained on an Agilent Technology LC/MSD trap SL instrument and a Thermo Scientific, LTQ Orbitrap XL™ high resolution system. The spectra of all compounds **1–4** were optimally run in the negative mode of ionization in water, with the exception of compounds **1** and **2**, the spectra of which were run in both negative and positive modes in methanol and/or water. In the case of compound **1**, 0.01% formic acid was added to the sample run in the positive mode in methanol.

3.6 Synthesis

3.6.1 Preparation of ligands L_iH_2 (i = 1–3). Ligands L_1H_2–L_3H_2 were prepared according to the literature.[32,34]

3.6.2 Preparation of complex $[VO(L_1)(CH_3O)(CH_3OH)]$ (1). To a solution of *o*-vanillin (0.15 g, 1.0 mmol) in CH_3OH (10 mL), 2-aminophenol (0.11 g, 1.0 mmol) was added under stirring. The resulting red solution was refluxed for two hours under continuous stirring and then it was cooled to room temperature. Subsequently, a solution of $[VO(C_5H_7O_2)_2]$ (0.27 g, 1.0 mmol) in CH_3OH (10 mL) was added under continuous stirring. The resulting slightly insoluble brownish reaction mixture was refluxed for an additional 2 h and then cooled to room temperature. Subsequently, the insoluble material was removed by filtration, the reaction flask with the clear reaction solution was placed at 4 °C, and diethyl ether was added. One week later, a brownish crystalline material precipitated at the bottom of the flask. The product was isolated by filtration and dried *in vacuo*. Yield: 0.22 g (58%). Anal. calcd for **1**, $[VO(L_1)(OCH_3)(CH_3OH)]$ (**1**). ($C_{16}H_{18}NO_6V$ M_r 371.25): C, 51.76; H, 4.89; N, 3.77. Found: C, 51.68; H, 4.79; N, 3.74.

3.6.3 Preparation of complex $[VO(L_1)(CH_3O)](C_{10}H_8N_2)[VO(L_1)(CH_3O)]$ (2). To a solution of *o*-vanillin (0.15 g, 1.0 mmol) in CH_3OH (10 mL), 2-aminophenol (0.11 g, 1.0 mmol) was added and the resulting red solution was refluxed for 2 h under continuous stirring. Then, it was cooled down to room temperature. Subsequently, a solution of $[VO(C_5H_7O_2)_2]$ (0.27 g, 1.0 mmol) in CH_3OH (10 mL) was added under continuous stirring. The resulting slightly insoluble brownish reaction mixture was refluxed for an additional 2 h and then cooled to room temperature. To that, a solution of 4,4′-bipyridine (0.16 g, 1.0 mmol) in CH_3OH (2 mL) was added under continuous stirring. The resulting insoluble brownish reaction mixture was refluxed for an additional 2 h and then cooled to room temperature. Subsequently, the insoluble material was removed by filtration, the reaction flask with the clear reaction solution was placed at 4 °C, and diethyl ether was added. Two weeks later, a brownish crystalline material precipitated at the bottom of the flask. The product was isolated by filtration and dried *in vacuo*. Yield: 0.14 g (33%). Anal. calcd for **2**, $[VO(L_1)(CH_3O)](C_{10}H_8N_2)[VO(L_1)(CH_3O)]$ (**2**). 2 × ($C_{20}H_{18}N_2O_5V$), M_r 2 × 417.31: C, 57.56; H, 4.35; N, 6.71. Found: C, 57.50; H, 4.33; N, 6.73.

3.6.4 Preparation of complex $[VO(L_2)(CH_3O)(CH_3OH)]$ (3). To a solution of salicylaldehyde (0.11 mL, 1 mmol) in CH_3OH (10 mL), 2-aminophenol (0.11 g, 1.0 mmol) was added and the resulting red solution was refluxed for 2 h. Then, it was cooled down to room temperature. Subsequently, a solution of $[VO(C_5H_7O_2)_2]$ (0.27 g, 1.0 mmol) in CH_3OH (10 mL) was added under continuous stirring and the resulting slightly insoluble brownish solution was refluxed for an additional 2 h. Then, it was cooled down to room temperature. Subsequently, the insoluble material was removed by filtration and the reaction flask with the clear reaction solution was placed at 4 °C to evaporate slowly. Ten days later, a brown crystalline material

precipitated at the bottom of the flask. The product was isolated by filtration and dried *in vacuo*. Yield: 0.19 g (55%). Anal. calcd for **3**, $[VO(L_2)(CH_3O)(CH_3OH)]$ (**3**). ($C_{15}H_{16}NO_5V$, M_r 341.24): C, 52.80; H, 4.73; N, 4.10. Found: C, 52.75; H, 4.70; N, 4.12.

3.6.5 Preparation of complex $[VO_2(L_3)Na(H_2O)_2VO_2(L_3)Na(H_2O)_3]_2{\cdot}H_2O$ (4). To a solution of 2-hydroxy-1-naphthaldehyde (0.17 g, 1.0 mmol) in CH_3OH (10 mL), 2-aminophenol (0.11 g, 1.0 mmol) was added and the resulting red solution was refluxed for 2 h at 70 °C. Then, it was cooled down to room temperature. Subsequently, a solution of $[VO(C_5H_7O_2)_2]$ (0.27 g, 1.0 mmol) in CH_3OH (10 mL) was added under continuous stirring and the resulting slightly insoluble brownish solution was refluxed for an additional 2 h. Then, it was cooled down to room temperature. Subsequently, sodium hydroxide (0.08 g, 2.0 mmol) was added to the reaction mixture under continuous stirring and the resulting clear, brownish solution was refluxed for an additional 2 h. Subsequently, the reaction flask was placed at 4 °C and allowed to evaporate slowly. One week later, a brown crystalline material precipitated at the bottom of the flask. The product was isolated by filtration and dried *in vacuo*. Yield: 0.19 g (45%). Anal. calcd for **4**, $[VO_2(L_3)Na(H_2O)_2VO_2(L_3)Na(H_2O)_3]_2{\cdot}H_2O$ (**4**). ($C_{68}H_{66}N_4Na_4O_{27}V_4$, M_r 1667.01): C, 48.99; H, 3.99; N, 3.36. Found: C, 49.01; H, 3.96; N, 3.38.

3.7 X-ray crystal structure determination

X-ray quality crystals of compounds **1** and **2** were grown from a mixture of methanol-diethyl ether, whereas crystals of compounds **3** and **4** were grown from methanol solutions. A crystal of **1** (0.03 × 0.05 × 0.30 mm) was recovered from the mother liquor and immediately cooled to −113 °C. Diffraction measurements were made on a Rigaku R-AXIS SPIDER Image Plate diffractometer using graphite monochromated Cu Kα radiation. Data collection (ω-scans) and processing (cell refinement, data reduction and empirical absorption correction) were performed using the CrystalClear program package.[49] The structures were solved by direct methods using SHELXS-97 and refined by full-matrix least-squares methods on F^2 with SHELXL2014/6.[50] Further experimental crystallographic details for **1**: $2\theta_{max}$ = 130.00°; 253 parameters refined; $(\Delta/\sigma)_{max}$ = 0.008; $(\Delta\rho)_{max}/(\Delta\rho)_{min}$ = 0.51/−0.48 e Å^{-3}. The hydrogen atoms were refined isotropically at positions located either from difference Fourier maps or at calculated positions using a riding model. All non-hydrogen atoms were refined anisotropically.

Crystals of **2**, **3**, and **4** suitable for X-ray diffraction, with dimensions 0.39 × 0.16 × 0.14 mm, 0.26 × 0.22 × 0.13 mm, and 0.53 × 0.14 × 0.06 mm, respectively, were taken from the mother liquor and mounted, at room temperature, on a Bruker Kappa 2 APEX diffractometer equipped with a triumph monochromator using Mo Kα radiation. Unit cell dimensions were determined and refined by using the angular settings of at least 100 high intensity reflections ($>10\sigma(I)$) in the range $15 < 2\theta < 40°$. Intensity data were recorded using ϕ and ω scans. All crystals exhibited no decay during data collection. The frames collected were integrated with the Bruker SAINT software package[51] using a narrow-frame algorithm. Data were corrected for absorption using the numerical method (SADABS) based on crystal dimensions.[52] Data refinement (full-matrix least-squares methods on F^2) and all subsequent calculations were performed using the Crystals version 14.61 build 6236 program package[53] The structures were solved by the SUPERFLIP method.[54] Molecular illustrations were drawn by Diamond 3.1c, CAMERON and Mercury crystallographic packages.[55] In all four structures **1–4**, all non-hydrogen atoms were refined anisotropically. Further experimental crystallographic details for **2**: θ_{max} = 33.178°; R/R_w (for all data), 0.0549/0.1113; for **3**: θ_{max} = 26.423°; R/R_w (for all data), 0.0810/0.1332; for **4**: θ_{max} = 27.442°; R/R_w (for all data), 0.0846/0.1183. Crystallographic details for **1–4** are summarized in Table 1.

3.8 Cell cultures and biological tests

3.8.1 Cell culture. Since the aim of the present study was to assess the adipogenic potential of the title V(v)-complexes, the established murine *in vitro* model 3T3-L1 (pre-adipocytes) was used. The specific cell line is insulin-sensitive and a common/ideal model of chemically induced differentiation to mature adipocytes. Both pre- and mature adipocytes were cultured in 75 cm^2 cell culture flasks under appropriate conditions (5% CO_2 at 37 °C and standard humidity) in Dulbecco's modified Eagle's medium, DMEM (Sigma, Steinheim, Germany). Culture media were supplemented with 10% Fetal Bovine Serum (FBS) (Biochrom, Berlin, Germany) and 1% penicillin–streptomycin (Biochrom, Berlin, Germany) prior to use. The specific cell line was tested and found free of mycoplasma contamination using a MycoAlert® Kit (Promega). All experiments were run at least in triplicate employing cells with a low passage number (P5–P9).

3.8.2 Chemically induced adipogenesis *in vitro*. Adipogenesis (maturation of pre-adipocytes into lipid droplet-containing adipocytes) was achieved by adding an appropriate adipogenic hormone cocktail (dexamethazone, isobutyl-methyl-xanthine, and insulin). 3T3-L1 fibroblasts were differentiated into mature adipocytes according to a standard differentiation protocol[56] as previously described. Briefly, two days post 70% confluency (day 0), cells were treated with 0.5 mM 3-isobutyl-1-methylxanthine (Sigma, Germany), 1.0 μM dexamethazone (Sigma, Steinheim, Germany), and 10 ng mL^{-1} of insulin as final concentrations in DMEM. Two days later (day 2), the cells were cultured in maintenance medium treated only with insulin (main adipogenic factor) and the medium was serially changed every two days. All experiments were performed on the 8th day of the differentiation process.

3.8.3 Cell viability assay. To examine cell survival rates post-stimulation with the well-characterized V(v)-complex species, both 3T3-L1 pre-adipocytes and mature adipocytes, differentiated with insulin as mentioned above, were seeded in 96-multi-well plates (2500 cells per well) and incubated with the title compounds for 24 and 48 h in DMEM. The employed assay relies on the quantitation of ATP present, thereby confirming the presence of metabolically active cells. The reagent (Promega kit Cell Titer-Glo®) is added to the cell culture (volumetric reagent/supernatant ratio 1 : 1) without removing the supernatant medium. The luminescence of each sample was measured on a GloMax® 96 Microplate Luminometer (Promega Corporation, WI USA). Results were expressed in relative percent change of luminescence

units (RLU). Cell viability was additionally tested *via* Trypan blue assay. Sodium deoxycholate (known cytotoxic agent) was used as positive control of the assay at a final concentration of 1 mg mL^{-1}.

3.8.4 Cell migration assay–cell morphology. Since the specific cell line exemplifies migrating characteristics, inhibition of the endogenous migrating capacity of 3T3-L1 pre-adipocytes was also assessed through an *in vitro* scratch assay.[57,58] For this purpose, cells were seeded in 35 mm cell culture dishes in DMEM. After achieving confluency (70–80%), (a) a scratch in the monolayer traversing the entire diameter of each culture dish was engraved using a sterile pipette tip, and (b) cells were allowed to grow in the culture medium, in the presence of a final concentration range of 1–20 μM of the title compounds. Cells were visualized using an Axio Observer Z1 microscope, with a 10× phase contrast objective (Carl Zeiss, GmbH Jena, Germany). Images were captured using an AxioCam Hc camera, at distinct time points (24 and 48 h) after the scratch had been made. Potential cytotoxic effects, in the presence of the materials tested, were also investigated with respect to cell morphology. Cells were regularly examined with respect to shape, appearance, color, confluency, *etc.*, to further confirm any aberration from the healthy status at several time points (prior and post treatment).

3.8.5 Induction of adipogenesis with V(v)-complexes. 3T3-L1 pre-adipocytes were differentiated into mature adipocytes following the standard differentiation protocol (*vide supra*) as described elsewhere.[59] 3T3-L1 fibroblast-like cells were treated with 10 ng mL^{-1} of insulin and/or selected well-defined vanadium complexes (1–20 μM). Vanadium complexes were dissolved in DMEM (10% FBS, 1% penicillin/streptomycin), followed by sterile filtration. In all experiments run, the insulin group was used as positive control. A control group with no treated cells (without insulin or vanadium complexes) was also included. On the 8th day of the differentiation process, cell differentiation was assessed with oil red O staining and Real-Time PCR for relative expression of closely related biomarkers. All tests were carried out at least in triplicate.

3.8.6 Oil red O staining. Successful cell differentiation into mature adipocytes was evaluated through oil red O staining, which was performed on the 8th day of the differentiation process. For that purpose, cells were washed with PBS (1×, pH 7.4) and fixed with 4% formalin for 20 min. Then, cells were washed with sterile doubly deionized water (ddH_2O) and treated with oil red O working solution for 15 min at room temperature. Subsequently, cells were washed with sterile ultrapure water and stained with hematoxylin for 1 min at room temperature. Cells were visualized using an Axio Observer Z1 microscope, with a 10× and 40× phase contrast objective (Carl Zeiss, GmbH Jena, Germany). Images were captured on an AxioCam Hc camera. All tests were carried out at least in triplicate.

3.8.7 RT-PCR assay. Total RNA was extracted from cells on the 8th day of the differentiation process, using Trizol (Life Science, Chemilab, Berkeley, California). Synthesis of cDNA was performed with the iScript cDNA synthesis kit (BioRad), according to the manufacturer instructions. RT-PCR was run on a Rotor Gene Q (Qiagen) using the QuantiTect SYBR Green PCR kit and appropriate reagents (Qiagen). The primers used were the following:

mGLUT4 forward 5′-AACCAGCATCTTCGAGTCGG-3′ and reverse 5′-TAAGAGCACCGAGACCAACG-3′;

mPPAR-γ forward 5′-GTCAGCGACTGGGACTTTTC-3′ and reverse 5′-CGAGGACATCCAAGACAACC-3′.

The sequence of each primer was run on BLAST to exclude those that would amplify undesired genes. Customized primers were also used from Qiagen for adiponectin (Mm_Adipoq_1_SG, NM_009605, Q01048047), resistin (Mm_Retn_1_SG, QT00093450) and insulin receptor (Mm_Insr_1_SG, NM_010568, QT00287903).

3.8.8 Statistical analysis. The data were presented as average and standard error mean (SEM) values of multiple sets of independent measurements. Mean survival rates and SEMs were calculated for each individual group. Absolute survival rates were calculated for each control group and one way analysis of variance (ANOVA) was performed for all pair comparisons, followed by *post hoc* analyses (Tukey) and Student *t* test in the case of RT-PCR experiments using GraphPad Prism v.6. Degrees of significance were assessed by three different rating values: $*p < 0.05$ (significant), $**p < 0.01$ (highly significant), $***p < 0.001$ (extremely significant) and $****p \leq 0.0001$ (extremely significant) or non-significant ($p > 0.05$).

4. Conclusions

Synthetic exploration of appropriately designed Schiff base ligands, extending from *o*-vanillin to salicylaldehyde and 2-hydroxy-1-naphthaldehyde cores and encompassing 2-aminophenolate tethers, with vanadyl acetylacetonate in methanolic solutions, led to crystalline materials **1–4**, bearing distinct molecular metal–ligand ratios, vanadium oxidation state and coordination composition as well as geometries. The physicochemical characterization in the solid state and in solution revealed the solid state–solution correlation profile, based on which further molecular biological studies, targeting their insulin mimetic potential in adipocyte differentiation, were pursued. The results (a) portray a well-described structure-specific behavior of vanadoforms inducing cellular differentiation, thus projecting the importance of that metal ion in adipogenesis, and (b) generate a well-defined molecular biological profile through genetic biomarkers pointing to potential metallopharmaceutical applications toward therapeutic interventions in Diabetes mellitus II (T2D).

Abbreviations

acac	Acetylacetonato
4,4′-bipy	4,4′-Bipyridine
DMEM	Dulbecco's modified Eagle's medium
EPR	Electron paramagnetic resonance
ESI-MS	Electron spray ionization-mass spectrometry
FBS	Fetal bovine serum
malto	Maltolato
ADIPOQ	Adiponectin
ANOVA	One way analysis of variance
DM	Diabetes mellitus
GLUT4	Glucose transporter 4

RETN	Resistin
INS-R	Insulin receptor
PBS	Phosphate buffer saline
PPAR-γ	Peroxisome proliferator-activated receptor gamma
SEM	Standard error mean

Conflicts of interest

There are no conflicts to declare.

References

1 A. Bradshaw Kaiser, N. Zhang and W. van der Pluijm, *Diabetes*, 2018, **67**(Suppl. 1), 202-LB.
2 A. T. Kharroubi and H. M. Darwish, *World J. Diabetes*, 2015, **6**, 850–867.
3 Z. T. Bloomgarden, *Diabetes Care*, 2007, **30**, 2737–2745.
4 K. Backholer, A. Peeters, W. H. Herman, J. E. Shaw, D. Liew, Z. Ademi and D. J. Magliano, *Diabetes Care*, 2013, **36**, 2714–2719.
5 H. M. Manukumar, J. S. Kumar, B. Chandrasekhar, S. Raghava and S. Umesha, *Crit. Rev. Food Sci. Nutr.*, 2017, **57**, 2712–2729.
6 (*a*) M. Brazil, *Nat. Rev. Drug Discovery*, 2002, **1**, 170; (*b*) N. Abirami, R. Arulmozhi and M. Sivakami, *Rec. Adv. Diabetes Treatment*, Avid Science, 2015, ch. 1, pp. 2–30; (*c*) J. J. Marín-Peñalver, I. Martín-Timón, C. Sevillano-Collantes and F. J. del Cañizo-Gómez, *World J. Diabetes*, 2016, **7**(17), 354–395.
7 V. V. Wong, K. W. Ho and M. G. Yap, *Cytotechnology*, 2004, **45**, 107–115.
8 E. L. Tolman, E. Barris, M. Burns, A. Pansisni and R. Partridge, *Life Sci.*, 1979, **25**, 1159–1164.
9 K. H. Thompson, Y. Tsukada, Z. Xu, M. Battell, J. H. McNeill and C. Orvig, *Biol. Trace Elem. Res.*, 2002, **86**, 31–44.
10 H. Sakurai, H. Yasui and Y. Adachi, *Expert Opin. Invest. Drugs*, 2003, **12**, 1189–1203.
11 K. H. Thomson, J. Lichter, C. LeBel, M. C. Scaife, J. H. McNeill and C. Orvig, *J. Inorg. Biochem.*, 2009, **103**, 554–558.
12 (*a*) N. Chasteen, *Struct. Bonding*, 1983, **53**, 105–138; (*b*) E. Irving and A. W. Stoker, *Molecules*, 2017, **22**(12), 2269; (*c*) C. C. McLauchlan, B. J. Peters, G. R. Willsky and D. C. Crans, *Coord. Chem. Rev.*, 2015, **301–302**, 163–199.
13 D. Rehder, *Inorg. Chem. Commun.*, 2003, **6**, 604–617.
14 A. M. A. Adam, A. M. Naglah, M. A. Al-Omar and M. S. Refat, *Int. J. Immunopathol. Pharmacol.*, 2017, **30**(3), 272–281.
15 M. C. Petersen and G. I. Shulman, *Physiol. Rev.*, 2018, **98**(4), 2133–2223.
16 K. Sarjeant and J. M. Stephens, *Cold Spring Harbor Perspect. Biol.*, 2012, **4**, a008417.
17 M. Coelho, T. Oliveira and R. Fernandes, *Arch. Med. Sci.*, 2013, **9**, 191–200.
18 M. Li, D. Wei, W. Ding, B. Baruah and D. C. Crans, *Biol. Trace Elem. Res.*, 2008, **121**, 226–232.
19 G. Scalese, I. Correia, J. Benítez, S. Rostán, F. Marques, F. Mendes, A. P. Matos, J. C. Pessoa and D. Gambino, *J. Inorg. Biochem.*, 2017, **166**, 162–172.
20 D. C. Crans, J. T. Koehn, S. M. Petry, C. M. Glover, A. Wijetunga, R. Kaur, A. Levina and P. A. Lay, *Dalton Trans.*, 2019, **48**, 6383–6395.
21 E. M. Zayed and M. A. Zayed, *Spectrochim. Acta, Part A*, 2015, **143**, 81–90.
22 E. Canpolat and M. Kaya, *J. Coord. Chem.*, 2004, **57**, 1217.
23 M. Yildiz, B. Dulger, S. Y. Koyuncu and B. M. Yapici, *J. Indian Chem. Soc.*, 2004, **81**, 7.
24 K. Singh, M. S. Barwa and P. Tyagi, *Eur. J. Med. Chem.*, 2007, **42**, 394.
25 P. G. Cozzi, *Chem. Soc. Rev.*, 2004, **33**, 410.
26 S. Chandra and J. Sangeetika, *J. Indian Chem. Soc.*, 2004, **81**, 203.
27 J. C. Pessoa, S. Etcheverry and D. Gambino, *Coord. Chem. Rev.*, 2015, **301–302**, 24–48.
28 I. Correia, I. Chorna, I. Cavaco, S. Roy, M. L. Kuznetsov, N. Ribeiro, G. Justino, F. Marques, T. Santos-Silva, M. F. A. Santos, H. M. Santos, J. L. Capelo, J. Doutch and J. C. Pessoa, *Chem. – Asian J.*, 2017, **12**, 2062.
29 I. E. Leon, J. F. Cadavid-Vargas, A. L. Di Virgilio and S. B. Etcheverry, *Curr. Med. Chem.*, 2017, **24**, 112–148.
30 T. Scior, J. A. Guevara-Garcia, Q. T. Do, P. Bernard and S. Laufer, *Curr. Med. Chem.*, 2016, **23**, 2874–2891.
31 (*a*) D. C. Crans, L. Henry, G. Cardiff and B. I. Posner, *Met. Ions Life Sci.*, 2019, **19**, 203–230; (*b*) M. Selman, C. Rousso, A. Bergeron, H. H. Son, R. Krishnan, N. A. El-Sayes, O. Varette, A. Chen, F. Le Boeuf, F. Tzelepis, J. C. Bell, D. C. Crans and J. S. Diallo, *Mol. Ther.*, 2018, **26**(1), 56–69.
32 R. Kannappan, D. M. Tooke, A. L. Spek and J. Reedijk, *Inorg. Chim. Acta*, 2006, **359**, 334–338.
33 J. Ondráček, Z. Kovárová, J. Maixner and F. Jursik, *Acta Crystallogr., Sect. C: Cryst. Struct. Commun.*, 1993, **49**, 1948–1949.
34 S. Das, *Polyhedron*, 2008, **27**, 517–522.
35 W. Chen, S. Gao and S. X. Liu, *Acta Crystallogr., Sect. C: Cryst. Struct. Commun.*, 1999, **55**, 531–533.
36 R. Bikas, H. H. Monfared, E. Jeanneau and B. Shaabani, *J. Chem.*, 2013, 546287.
37 E. Halevas, O. Tsave, M. P. Yavropoulou, A. Hatzidimitriou, J. G. Yovos, V. Psycharis, C. Gabriel and A. Salifoglou, *J. Inorg. Biochem.*, 2015, **147**, 99–115.
38 I. Correia, J. C. Pessoa, M. T. Duarte, M. F. Minas da Piedade, T. Jackush, T. Kiss, M. M. C. A. Castro, C. F. G. C. Geraldes and F. Avecilla, *Eur. J. Inorg. Chem.*, 2005, 732–744.
39 D. F. Evans and P. H. Missen, *J. Chem. Soc., Dalton Trans.*, 1987, 1279–1281.
40 S. M. El-Medani, O. A. M. Ali and R. M. Ramadan, *J. Mol. Struct.*, 2005, **738**, 171–177.
41 R. Dinda, P. Sengupta, S. Ghosh and T. C. W. Mak, *Inorg. Chem.*, 2002, **41**, 1684–1688.
42 C. Duval, *Inorganic Thermogravimetric Analysis*, Elsevier Publishing Co., Amsterdam, Second and Revised Edition, 1963.
43 J. Janke, S. Engeli, K. Gorzelniak, F. C. Luft and A. M. Sharma, *Obes. Res.*, 2002, **10**, 1–5.
44 Y. Ikeda, H. Tsuchiya, S. Hama, K. Kajimoto and K. Kogure, *FEBS J.*, 2013, **280**, 5884–5895.

45 C. Bulcão, S. R. Ferreira, F. M. Giuffrida and F. F. Ribeiro-Filho, *Curr. Diabetes Rev.*, 2006, **2**, 19–28.
46 M. E. Trujillo and P. E. Scherer, *J. Intern. Med.*, 2005, **257**, 167–175.
47 K. Bäck and H. J. Arnqvist, *Growth Horm. IGF Res.*, 2009, **19**, 101–111.
48 M. E. Fernyhough, E. Okine, G. Hausman, J. L. Vierck and M. V. Dodson, *Domest. Anim. Endocrinol.*, 2007, **33**, 367–378.
49 Rigaku/MSC, CrystalClear, Rigaku/MSC Inc., The Woodlands, Texas, USA, 2005.
50 (*a*) G. M. Sheldrick, *Acta Crystallogr., Sect. A: Found. Crystallogr.*, 2008, **64**, 112–122; (*b*) G. M. Sheldrick, *Acta Crystallogr., Sect. C: Struct. Chem.*, 2015, **71**, 3–8.
51 Bruker Analytical X-ray Systems, Inc. Apex2, Version2 User Manual, M86-E01078, Madison, WI, 2006.
52 Siemens Industrial Automation, Inc. SADABS: Area-Detector Absorption Correction; Madison, WI, 1996.
53 L. Palatinus and G. J. Chapuis, *Appl. Crystallogr.*, 2007, **40**, 786–790.
54 P. W. Betteridge, J. R. Carruthers, R. I. Cooper, K. Prout and D. J. Watkin, *J. Appl. Crystallogr.*, 2003, **36**, 1487.
55 (*a*) DIAMOND – Crystal and Molecular Structure Visualization, Ver. 3.1c, Crystal Impact, Rathausgasse 30, 53111, Bonn, Germany; (*b*) D. J. Watkin, C. K. Prout and L. J. Pearce, *CAMERON*, Chemical Crystallography Laboratory, Oxford, UK, 1996; (*c*) Mercury CSD 2.0 – New Features for the Visualization and Investigation of Crystal Structures, Cambridge Crystallographic Data Centre, 2017; (*d*) C. F. Macrae, I. J. Bruno, J. A. Chisholm, P. R. Edgington, P. McCabe, E. Pidcock, L. Rodriguez-Monge, R. Taylor, J. van de Streek and P. A. Wood, *J. Appl. Crystallogr.*, 2008, **41**, 466–470.
56 O. Tsave, E. Halevas, M. P. Yavropoulou, A. Kosmidis Papadimitriou, J. G. Yovos, A. Hatzidimitriou, C. Gabriel, V. Psycharis and A. Salifoglou, *J. Inorg. Biochem.*, 2015, **152**, 123–137.
57 O. Tsave, M. P. Yavropoulou, M. Kafantari, C. Gabriel, J. G. Yovos and A. Salifoglou, *J. Inorg. Biochem.*, 2016, **163**, 323–331.
58 C. C. Liang, A. Y. Park and J. L. Guan, *Nat. Protoc.*, 2007, **2**, 2.
59 O. Tsave, M. P. Yavropoulou, M. Kafantari, C. Gabriel, J. G. Yovos and A. Salifoglou, *J. Inorg. Biochem.*, 2018, **186**, 217–227.

